Marginal stability, characteristic frequencies, and growth rates of gradient drift modes in partially magnetized plasmas with finite electron temperature

V. P. Lakhin, V. I. Ilgisonis, A. I. Smolyakov, E. A. Sorokina, and N. A. Marusov

Citation: Physics of Plasmas **25**, 012107 (2018); doi: 10.1063/1.4996719
View online: https://doi.org/10.1063/1.4996719
View Table of Contents: http://aip.scitation.org/toc/php/25/1
Published by the American Institute of Physics

PHYSICS OF PLASMAS 25, 012107 (2018)

Marginal stability, characteristic frequencies, and growth rates of gradient drift modes in partially magnetized plasmas with finite electron temperature

V. P. Lakhin,[1,2] V. I. Ilgisonis,[2,3] A. I. Smolyakov,[1,2,4] E. A. Sorokina,[1,2] and N. A. Marusov[1,2,5]
[1]*NRC "Kurchatov Institute", 1 Kurchatov Sq., Moscow, 123182, Russia*
[2]*Peoples' Friendship University of Russia (RUDN University), 3 Ordzhonikidze St., Moscow, 117198, Russia*
[3]*State Atomic Energy Corporation ROSATOM, 24 Bolshaya Ordynka St., Moscow, 119017, Russia*
[4]*University of Saskatchewan, 116 Science Place, Saskatoon, SK S7N 5E2, Canada*
[5]*Moscow Institute of Physics and Technology, 9 Institutskiy per., Dolgoprudny, 141701, Russia*

(Received 18 July 2017; accepted 14 November 2017; published online 5 January 2018)

The detailed analysis of stability of azimuthal oscillations in partially magnetized plasmas with crossed electric and magnetic fields is presented. The instabilities are driven by the transverse electron current which, in general, is due to a combination of $\mathbf{E}\times\mathbf{B}$ and electron diamagnetic drifts. Marginal stability boundary is determined for a wide range of the equilibrium plasma parameters. It is shown that in some regimes near the instability threshold, only the low-frequency long-wavelength oscillations are unstable, while the short-wavelength high-frequency modes are stabilized by the finite Larmor radius effects. Without such stabilization, the high-frequency modes have much larger growth rates and dominate. A new regime of the instability driven exclusively by the magnetic field gradient is identified. Such instability takes place in the region of the weak electric field and for relatively large gradients of plasma density ($\rho_s/l_n > 1$, where ρ_s is the ion-sound Larmor radius and l_n is the scale length of plasma density inhomogeneity). *Published by AIP Publishing.* https://doi.org/10.1063/1.4996719

I. INTRODUCTION

Partially magnetized plasma in crossed electric and magnetic fields is subject to gradient drift instabilities[1–7] which are driven by the azimuthal equilibrium electron flow. Such instabilities are of interest for a number of applications in electric propulsion devices, magnetic filters, and plasma processing devices.[8–13] In this paper, we present the results of a detailed quantitative analysis of plasma stability with respect to azimuthal perturbations for a wide range of equilibrium plasma parameters taking into account finite electron temperature effects. The free energy source of instability is provided by the electron flow across the magnetic field which is a combination of the electron $\mathbf{E}\times\mathbf{B}$ and the diamagnetic drifts. In the latter, the compressible part parameterized by the electron magnetic drift velocity V_D plays the key role. Overall, the instability is controlled by the inhomogeneities of plasma density and the magnetic field. We show that, in general, the characteristics of the instability are defined by the three dimensionless parameters characterizing the plasma equilibrium (see Sec. II). These parameters are proportional to the equilibrium azimuthal electron drift, the plasma density gradient, and the magnetic field gradient. We analyse plasma stability separately in the case of moderate and strong electric field $V_E \gtrsim V_D$ (Sec. III) and for a somewhat special case of negligibly weak electric field, $V_E \ll V_D$ (Sec. IV). As it is shown below, the instability is possible only inside a finite interval of the magnetic drift velocity limited both from below and from above.

It has been shown in Ref. 14 that the threshold value of the electron drift velocity for the instability depends on the wavenumber of perturbations. Here, we derive analytically the minimal value of the instability drive for all possible ranges of equilibrium plasma parameters. The investigation of the marginal stability conditions is of interest in relation to the concept of the self-organized criticality of the anomalous transport in which it is assumed that the plasma organizes itself into the state in which the plasma parameters are maintained at marginal stability.[15–17] Such anomalous transport driven by the gradient drift modes was studied in Refs. 15–17 in application to open-mirror systems. In application to the Hall thruster, the marginal stability due to gradient-drift modes and some experimental evidence were discussed in Ref. 3.

When the instability drive exceeds the critical value, the oscillations with the largest growth rate take place and dominate. Therefore, in Secs. III and IV, we analyze the maximal growth rates of oscillations and corresponding to them frequencies for all ranges of the equilibrium plasma parameters for strong and negligibly weak electric field, respectively. We combine some analytical studies with numerical calculations. In Sec. V, the conclusions are presented.

II. DISPERSION RELATION

The gradient drift instabilities are studied here employing the two-fluid model. We restrict ourselves to the electrostatic perturbations with the frequency ω in the range $\omega_{Bi} \ll \omega \ll \omega_{Be}$ and with the wavevector $\mathbf{k}$ perpendicular to the external magnetic field such that $\omega \gg kv_{Ti}$, where $\omega_{B\alpha}$, $\alpha=(i,e)$ are the ion and electron cyclotron frequencies, $v_{Ti}=(2T_i/m_i)^{1/2}$ is the ion thermal velocity, and T_i, m_i are the ion temperature and mass.

Under the above assumptions, the ions are unmagnetized and cold. They are described by the following equations:

$$\frac{\partial \mathbf{v}_i}{\partial t} + (\mathbf{v}_i \cdot \nabla)\mathbf{v}_i = -\frac{e}{m_i}\nabla\phi, \tag{1}$$

$$\frac{\partial n_i}{\partial t} + \nabla \cdot (n_i \mathbf{v}_i) = 0. \tag{2}$$

Here, $\mathbf{v}_i$ and n_i are the ion velocity and density, ϕ is the electric potential, and e is the proton charge.

To describe the electron density, we use the following equation:

$$\begin{aligned}&\left(\frac{\partial}{\partial t} + \mathbf{V}_E \cdot \nabla\right) n_e - 2n_e(\mathbf{V}_E + \mathbf{V}_p)\cdot \nabla \ln B_0 \\ &+ \nabla_\perp^2\left(\frac{n_e T_e}{m_e \omega_{Be}^2}(\mathbf{V}_E + \mathbf{V}_p)\cdot\nabla \ln B_0\right) - \frac{1}{m_e\omega_{Be}} \\ &\times \left\{\nabla\left(\frac{n_e T_e}{\omega_{Be} B_0}\nabla\cdot((\mathbf{V}_E+\mathbf{V}_p)\times \mathbf{B}_0)\right)\times \mathbf{b}\right\}\cdot \nabla \ln B_0 \\ &+ \nabla\cdot\left\{\frac{n_e}{\omega_{Be}}\left[\left(\frac{\partial}{\partial t} + (\mathbf{V}_E + \mathbf{V}_D)\cdot\nabla\right)(\mathbf{V}_E + \mathbf{V}_p)\right]\times \mathbf{b}\right\} = 0.\end{aligned} \tag{3}$$

Here,

$$\mathbf{V}_E = \frac{c}{B_0}\mathbf{b}\times\nabla\phi, \quad \mathbf{V}_p = \frac{cT_e}{en_eB_0}\nabla n_e \times \mathbf{b},$$
$$\mathbf{V}_D = \frac{2cT_e}{eB_0}\nabla \ln B_0 \times \mathbf{b},$$

where c is the speed of light, m_e is the mass of electron, B_0 is the equilibrium magnetic field, and $\mathbf{b} \equiv \mathbf{B}_0/B_0$. The electron temperature $T_e = p_e/n_e$ is assumed to be homogeneous and its perturbation is neglected; p_e and n_e are the electron pressure and density, respectively. The magnetic field is created by the external coils, so that in plasma $\nabla \times \mathbf{B}_0 = 0$. This electron continuity equation has been derived in Refs. 14 and 18 and includes the finite Larmor radius (FLR) effects in the Padé approximation and the effects of the external magnetic field inhomogeneity.

We suppose that the plasma density is sufficiently high so that $\omega_{pe} \gg \omega_{Be}$ (ω_{pe} is the electron Langmuir frequency) and close the set of Eqs. (1)–(3) with the quasineutrality condition

$$n_e = n_i. \tag{4}$$

We assume that the plasma is in the external crossed electric in the x-direction $\mathbf{E}_0 = -(d\phi_0(x)/dx)\mathbf{e}_x$ and the magnetic field predominantly in the z-direction $\mathbf{B}_0 = B_{0x}\mathbf{e}_x + B_{0z}\mathbf{e}_z$, $B_{0z} \gg B_{0x}$. Then in steady state, the magnetized electrons move in the azimuthal y-direction with the velocity

$$\mathbf{v}_{0e} = (V_E + V_{\star e})\mathbf{e}_y, \quad V_E = -\frac{c}{B_0}E_0 = \frac{c}{B_0}\frac{d\phi_0}{dx},$$
$$V_{\star e} = -\frac{cT_e}{eB_0}\frac{d\ln n_{0e}}{dx}.$$

We restrict ourselves to almost azimuthal oscillations, such that $k_y \gg k_x$ and neglect the effect of steady-state ion flow in the direction of electric field $\mathbf{E}_0$. Then, linearizing Eqs. (1)–(4) with respect to small-amplitude perturbations proportional to $\exp(-i\omega t + ik_x x + ik_y y)$, we arrive at the following local dispersion relation:

$$\begin{aligned}&1 - \frac{\omega_{lh}^2(1+k_\perp^2\rho_e^2)}{\omega^2} + \frac{1}{k_\perp^2\rho_e^2} \\ &\times \frac{\omega_{\star e}(1+k_\perp^2\rho_e^2) - \omega_D(1+2k_\perp^2\rho_e^2)}{(\omega-\omega_E)(1+k_\perp^2\rho_e^2) - \omega_D(1+2k_\perp^2\rho_e^2)} = 0.\end{aligned} \tag{5}$$

Here, $\omega_{lh} = (\omega_{Be}\omega_{Bi})^{1/2}$ is the lower-hybrid frequency, $\rho_e = (T_e/m_e\omega_{Be}^2)^{1/2}$ is the electron Larmor radius, and

$$(\omega_{\star e}, \omega_E, \omega_D) = k_y(V_{\star e}, V_E, V_D), \quad V_D = -\frac{2cT_e}{eB_0}\kappa_B$$

are the electron diamagnetic drift, the $\mathbf{E}_0 \times \mathbf{B}_0$-drift, and the electron magnetic drift frequencies, respectively; $(\kappa_n, \kappa_B) = d\ln(n_0, B_0)/dx$ are the characteristic variation lengths of the equilibrium plasma density and magnetic field magnitude, and $k_\perp^2 \equiv k_x^2 + k_y^2$.

This dispersion relation (5) follows from the more general equation derived earlier.[14] Simplifications were made based on the following assumptions: (1) the plasma is dense, so that $\omega_{pe}^2/\omega_{Be}^2 \gg 1$; (2) the oscillations are almost azimuthal, $k_y \gg k_x$, and the effect of steady-state ion flow in the direction of electric field $\mathbf{E}_0$ is neglected; (3) the wavelength of oscillations is large compared to the electron Debye length $d_e = (T_e/m_e\omega_{pe}^2)^{1/2}$, $k_\perp^2 d_e^2 \ll 1$. Dispersion relation (5) takes into account the electron inertia effects represented by the first term 1 and the electron finite Larmor radius effects in the Padé approximation terms proportional to $k_\perp^2\rho_e^2$ in combinations with 1.

For the further analysis, we represent the dispersion relation in the dimensionless form

$$\Omega^3 + \lambda\sigma\Omega^2 - \Omega - \sigma = 0, \tag{6}$$

where

$$\begin{aligned}&\Omega \equiv \omega/\omega_0, \; k \equiv k_\perp\rho_e, \; \omega_0 = \omega_{lh}(1+k^2)^{1/2}, \\ &\lambda = 1 - \frac{1}{k^2}\cdot\frac{(1+k^2)\chi_n - (1+2k^2)\chi_B}{(1+k^2)\xi + k^2\chi_B}, \\ &\sigma = \frac{k\cos\theta}{(1+k^2)^{3/2}}\cdot\left[(1+k^2)\xi + k^2\chi_B\right], \\ &\xi = -\frac{V_E + V_D}{c_s}, \quad \chi_n = -\frac{V_{\star e}}{c_s} \equiv \rho_s\kappa_n, \quad \chi_B = -\frac{V_D}{c_s} \equiv 2\rho_s\kappa_B,\end{aligned} \tag{7}$$

where $c_s = (T_e/m_i)^{1/2}$ is the ion-sound speed, $\rho_s = c_s/\omega_{Bi}$ is the ion-sound Larmor radius, and $\cos\theta = k_y/k_\perp$. Restricting ourselves to the azimuthal oscillations below, we put $|\cos\theta| = 1$. The parameter ξ is proportional to perpendicular equilibrium electron current $V_E + V_D$—the source of free energy—and characterizes the "drive" of gradient drift instability. The parameters χ_n and χ_B in the numerator of λ correspond to plasma density and magnetic field inhomogeneities which play the role of the instability trigger. It was shown in Ref. 14 that the necessary instability condition for gradient-drift modes described by Eq. (6) is $\lambda < 1$; we will use this condition below.

To simplify the subsequent study of instability, it is useful to notice that the dispersion relation is symmetrical with respect to the transformation

$$\xi \to -\xi,\ \chi_n \to -\chi_n,\ \chi_B \to -\chi_B,\ k_y \to -k_y. \tag{8}$$

It means that for studying the instability one can fix the sign of one of the parameters, e.g., $\chi_n > 0$.

III. GRADIENT DRIFT INSTABILITY FOR STRONG ELECTRIC FIELD, $|V_E/V_D| \gtrsim 1$

Assuming that $|V_E/V_D| \gtrsim 1$, we start from the general case of dispersion relation (5). The oscillations are characterized by three *independent* equilibrium parameters—ξ, χ_n, and χ_B, and the value of the wavenumber k.

A. Instability region and marginal stability condition

According to the analysis presented in Ref. 14, the necessary instability condition is $\lambda < 1$ or

$$\frac{(1+k^2)\chi_n - (1+2k^2)\chi_B}{(1+k^2)\xi + k^2\chi_B} > 0. \tag{9}$$

Then, taking into account the above noted property of the dispersion relation described by Eq. (8), we fix $\chi_n > 0$ and consider variations of another two equilibrium parameters—ξ and χ_B.

For $\chi_n > 2\chi_B$, the numerator of fraction in inequality (9) is positive for any k^2; for $\chi_B > \chi_n$, it is negative for any k^2, and for $\chi_n/2 < \chi_B < \chi_n$, it changes sign at $k^2 = k_\star^2$. The defining wavenumber $k_\star^2$ is

$$k_\star^2 = \frac{\chi_n - \chi_B}{2\chi_B - \chi_n}. \tag{10}$$

Therefore, we separate the whole interval of the parameter χ_B into 3 subintervals: (a) $-\infty < \chi_B \le \chi_n/2$; (b) $\chi_n/2 < \chi_B < \chi_n$; (c) $\chi_B \ge \chi_n$. Then the necessary instability condition (9) in the subinterval (a) is satisfied if

$$\xi > -\frac{k^2}{(1+k^2)}\chi_B, \tag{11}$$

in the subinterval (b) if

$$\begin{cases} \xi > -k^2\chi_B/(1+k^2), & \text{for } k^2 < k_\star^2; \\ \xi < -k^2\chi_B/(1+k^2), & \text{for } k^2 > k_\star^2, \end{cases} \tag{12}$$

and in the subinterval (c) if

$$\xi < -\frac{k^2}{(1+k^2)}\chi_B. \tag{13}$$

The corresponding regions of possible instability are presented in Fig. 1.

The instability boundary is determined by the zero value of the determinant of Eq. (6), which gives the equation

$$F \equiv 4\lambda^3\sigma^4 + (\lambda^2 + 18\lambda - 27)\sigma^2 + 4 = 0, \tag{14}$$

and the necessary and sufficient instability condition has the form

$$\begin{cases} \sigma^2 > \mu_1, & \text{for } \lambda \le 0; \\ \mu_1 < \sigma^2 < \mu_2, & \text{for } 0 < \lambda < 1, \end{cases} \tag{15}$$

where

$$\mu_{1,2} = \frac{1}{8\lambda^3}\left[27 - 18\lambda - \lambda^2 \mp \sqrt{(1-\lambda)(9-\lambda)^3}\right]. \tag{16}$$

The details of the derivation of instability condition (15) can be found in Ref. 14.

As it is already mentioned in the Introduction, the gradient-drift instability is driven by the equilibrium plasma current perpendicular to the magnetic field and arises when this current exceeds some critical value. Therefore, it is important to know this value. In our representation, the instability drive is associated with the parameter ξ. Its minimal value can be found by a minimization of ξ with respect to the wavenumber k^2 on the instability boundary in the interval $0 < k^2 < \infty$. We consider Eq. (14), $F = 0$, as the equation defining the implicit function $\xi = \xi(k^2)$ at fixed values of parameters χ_n and χ_B. Then, the function ξ has the extremum either at the stationary points defined by the set of equations

$$\frac{\partial F}{\partial k^2} = 0,\ \ F = 0, \tag{17}$$

or at the edge points of the interval.

Solving Eqs. (17), we find that inside the instability region these equations describe only two possible stationary points. One of them is described by the set of equations

$$k_1^2 = \frac{\chi_n - \chi_B - \xi}{2(2\chi_B - \chi_n)},\ \ (\xi + \chi_n - \chi_B)^2 = 1, \tag{18}$$

and the other one by the equations

$$k_2^2 = \frac{\xi - \chi_B}{\xi + \chi_B}\cdot\frac{\chi_n - \chi_B}{2\chi_B - \chi_n},\quad (\xi + \chi_B)^2 = \frac{\chi_B}{\chi_n - \chi_B}. \tag{19}$$

Of course, the corresponding stationary point does exist only for such χ_n and χ_B that the solution of equations satisfies the following two conditions: (1) ξ is a real value; (2) $k_i^2 \ge 0$, $i = (1,2)$.

Also, we find that for small k^2 such that $k^2 \ll 1$ the lower branch of instability boundary, $\sigma^2 = \mu_1$, takes the form

$$\xi = \frac{1}{4(\chi_n - \chi_B)}\left\{1 + (4\chi_B(\chi_n - \chi_B) - 1) \times \left(\frac{1}{4(\chi_n - \chi_B)^2} - 1\right)k^2 + O(k^4)\right\}. \tag{20}$$

Thus, for long-wavelength oscillations with $k^2 \to 0$, the instability boundary is defined by the expression

$$\xi = \frac{1}{4(\chi_n - \chi_B)} \equiv \xi_0. \tag{21}$$

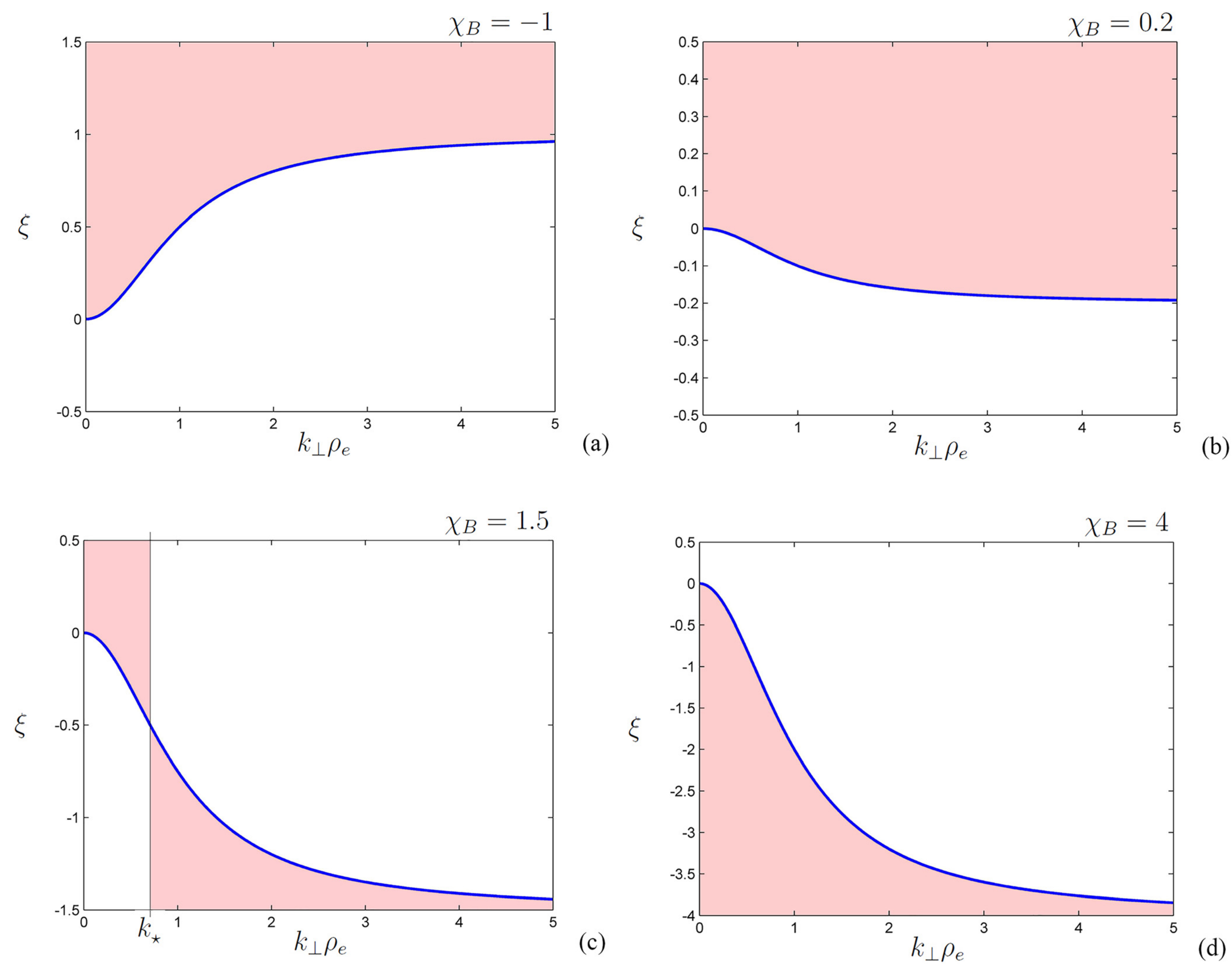

FIG. 1. Necessary instability condition in (k, ξ)-plane for fixed χ_n (namely, $\chi_n = 2$) and different χ_B: (a) $\chi_B \leq 0$ (namely, $\chi_B = -1$); (b) $0 < \chi_B \leq \chi_n/2$ (namely, $\chi_B = 0.2$); (c) $\chi_n/2 < \chi_B < \chi_n$ (namely, $\chi_B = 1.5$); and (d) $\chi_B \geq \chi_n$ (namely, $\chi_B = 4$). The region of possible instability is shaded.

Now let us study the instability region for the above three subintervals of parameter χ_B.

1. $-\infty < \chi_B \leq \chi_n/2$

In this interval of χ_B, we have $2\chi_B - \chi_n < 0$. Therefore, according to Eq. (18), one of possible stationary points is defined by the following expressions:

$$\xi = 1 - \chi_n + \chi_B \equiv \xi_{1+}, \quad k^2 = \frac{1}{2} \cdot \frac{1 - 2(\chi_n - \chi_B)}{\chi_n - 2\chi_B} \equiv k_{1+}^2. \tag{22}$$

In fact, this point can exist ($k^2 \geq 0$) only in the interval

$$\chi_n - 1/2 < \chi_B \leq \chi_n/2. \tag{23}$$

These inequalities are compatible if $\chi_n < 1$. Therefore, the stationary point (ξ_{1+}, k_{1+}) takes place if the parameters χ_n and χ_B belong to the region: $\chi_n - 1/2 < \chi_B \leq \chi_n/2$ and $\chi_n < 1$.

In accordance with Eq. (19), another possible stationary point can exist only in the subinterval $0 < \chi_B < \chi_n/2$. It is described by the equations

$$\xi = \sqrt{\frac{\chi_B}{\chi_n - \chi_B}} - \chi_B \equiv \xi_{2+},$$
$$k^2 = \frac{\chi_n - \chi_B}{\chi_n - 2\chi_B} \cdot \left[2\sqrt{\chi_B(\chi_n - \chi_B)} - 1\right] \equiv k_{2+}^2. \tag{24}$$

This stationary point (ξ_{2+}, k_{2+}) takes place, $k^2 > 0$, only for $\chi_n > 1$ and

$$\chi_B^{(-)} < \chi_B \leq \frac{1}{2}\chi_n, \quad \text{where } \chi_B^{(-)} \equiv \frac{1}{2}\left(\chi_n - \sqrt{\chi_n^2 - 1}\right). \tag{25}$$

Now, let us consider the minimization of ξ with respect to k for two intervals of parameter χ_n.

For $\chi_n < 1$ and $-\infty < \chi_B \leq \chi_n - 1/2$, there are no stationary points of ξ in the interval $0 < k < \infty$. According to expression (20) in the vicinity of $k = 0$, the function ξ is the growing function of k. At $k \to \infty$, the function ξ on the instability boundary asymptotically approaches the value $\xi_\infty^{(+)}$

$$\xi \to \xi_\infty^{(+)} \equiv 1 - \chi_B. \tag{26}$$

Thus, on the lower branch of instability boundary, ξ is the growing function of k everywhere in the interval $0 < k < \infty$. Thus, in the discussed range of plasma parameters, the instability threshold has its minimum at $k \to 0$. Hereafter, we call the value of ξ on the instability boundary minimized with respect to k, *the critical value of instability drive* ξ_{cr}. So, in this range of parameters, $\xi_{cr} = \xi_0$.

For $\chi_n < 1$ and $\chi_n - 1/2 < \chi_B \le \chi_n/2$, the function ξ is the decreasing function of k in the vicinity of $k=0$. It reaches the minimum at the stationary point $k = k_{1+}$, and, therefore, $\xi_{cr} = 1 - \chi_n + \chi_B$. With the further increase of k in the interval $k_{1+} < k < \infty$, the lower branch of instability boundary goes to $\xi_\infty^{(+)}$. With the increase of χ_B, the point of minimal threshold k_{1+} shifts from the long-wavelength oscillations with $k=0$ (at $\chi_B = \chi_n - 1/2$) to the short-wavelength modes with $k \to \infty$ (at $\chi_B \to \chi_n/2$). The frequency of the marginally stable mode also increases with the increase of χ_B.

For $\chi_n > 1$ and $-\infty < \chi_B < \chi_B^{(-)}$, the function ξ on the lower branch of instability boundary is the increasing function of k for any $0 < k < \infty$ and therefore $\xi_{cr} = \xi_0$.

For $\chi_n > 1$ and $\chi_B^{(-)} < \chi_B \le \chi_n/2$, the function ξ has its minimum for the oscillations with $k = k_{2+}$ and the critical value of instability drive is $\xi_{cr} = \xi_{2+}$. The value of k_{2+} increases from $k_{2+} = 0$ (at $\chi_B^{(-)}$) to $k_{2+} \to \infty$. It means that with the increase of χ_B the oscillations with the minimal threshold have more and more short wavelength and high frequency.

2. $\chi_n/2 < \chi_B < \chi_n$

For χ_B belonging to this interval, the necessary instability condition changes its sign depending on the magnitude of the wavenumber. For the oscillations with $k < k_\star$, the necessary instability condition is $(1 + k^2)\xi + k^2\chi_B > 0$. For the shorter-wavelength oscillations, $k > k_\star$, the necessary instability condition is $(1 + k^2)\xi + k^2\chi_B < 0$.

a. Oscillations with $k \le k_\star$. For such oscillations with $k \le k_\star$, the stationary point described by Eq. (18) in the interval $k < k_\star$ does exist only for $\chi_n > 1$ and $\chi_n/2 < \chi_B < \chi_n - 1/2$. It is described by expressions $\xi = \xi_{1+}$ and $k = k_{1+}$.

Another possible stationary point defined by Eq. (19) is characterized by $\xi = \xi_{2+}$ and $k = k_{2+}$. For $\chi_n \le 1$, such a point does exist for any χ_B from the interval $\chi_n/2 < \chi_B < \chi_n$. For $\chi_n > 1$, it does exist only if

$$\chi_B^{(+)} < \chi_B < \chi_n, \quad \text{where} \quad \chi_B^{(+)} \equiv \frac{1}{2}\left[\chi_n + \sqrt{\chi_n^2 - 1}\right].$$

Thus, for $\chi_n \le 1$, the function ξ on the lower branch of instability boundary starts from the point $\xi = \xi_0$ at $k \to 0$ and decreases with the increase of k up to $k = k_{2+}$. It reaches the minimum for the oscillations with $k = k_{2+}$. This critical value is $\xi_{cr} = \xi_{2+}$. With further increase of k in the interval $k_{2+} < k \le k_\star$, the function ξ grows and reaches the value

$$\xi = \chi_B - \chi_n + \sqrt{\frac{\chi_B}{\chi_B - \chi_n}} \equiv \xi_\star^{(+)}$$

at $k = k_\star$. At the point $(\xi_\star^{(+)}, k_\star)$, the lower branch of instability boundary intersects with the upper one defined by the equation $\sigma^2 = \mu_2$. The value of ξ_{cr} increases with the growth of χ_B from $1 - \chi_n/2$ (at $\chi_B = \chi_n/2$) to ∞ (when $\chi_B \to \chi_n$) and the minimal threshold point k_{2+} shifts from the short-wavelength high-frequency oscillations with

$$k \to \frac{\chi_n(1 - \chi_n)}{2(2\chi_B - \chi_n)} \to \infty, \quad \text{at} \quad \chi_B \to \chi_n/2,$$

to the long-wavelength ($k \to 0$) low-frequency modes at $\chi_B \to \chi_n$.

Now, let us analyze the case $\chi_n > 1$. For $\chi_n/2 < \chi_B < \chi_n - 1/2$, the function ξ on the lower instability boundary reaches its minimum for the oscillations with $k = k_{1+}$ and therefore $\xi_{cr} = \xi_{1+}$. For $\chi_B \to \chi_n/2$, the lowest threshold corresponds to the short-wavelength high-frequency oscillations with

$$k \to \frac{\chi_n - 1}{2(2\chi_B - \chi_n)} \to \infty, \quad \text{at} \quad \chi_B \to \chi_n/2.$$

With the increase of χ_B, the point $k = k_{1+}$ shifts towards long wavelengths and $k_{1+} \to 0$ at $\chi_B = \chi_n - 1/2$. When $\chi_n - 1/2 \le \chi_B \le \chi_B^{(+)}$, the function ξ on the lower branch of instability boundary is the increasing function of k for $0 < k \le k_\star$. The lowest instability threshold corresponds to the longest-wavelength oscillations with $k \to 0$ and the critical instability drive is $\xi_{cr} = \xi_0$. Finally, for $\chi_B^{(+)} < \chi_B < \chi_n$, the lowest threshold $\xi_{cr} = \xi_{2+}$ corresponds to the oscillations with $k = k_{2+}$. The numerical calculations show that with the increase of χ_B the function k_{2+} starting from $k_{2+} = 0$ at $\chi_B = \chi_B^{(+)}$ increases and reaches its maximum approximately in the center of the interval at $\chi_B \approx (\chi_B^{(+)} + \chi_n)/2$ and decreases with further increase of χ_B so that $k_{2+} \to 0$ at $\chi_B \to \chi_n$.

b. Oscillations with $k > k_\star$. For the oscillations with $k > k_\star$, there are two stationary points on the instability boundary. The first one takes place at $k = k_{1-}$ on the lower branch of instability boundary $\sigma^2 = \mu_1$ and corresponds to its maximum $\xi = \xi_{1-}$, where

$$k_{1-}^2 = \frac{1 + 2(\chi_n - \chi_B)}{2(2\chi_B - \chi_n)}, \quad \xi_{1-} = \chi_B - \chi_n - 1. \tag{27}$$

The second stationary point takes place at $k = k_{2-}$ on the upper branch of instability boundary $\sigma^2 = \mu_2$ and corresponds to its minimum $\xi = \xi_{2-}$, where

$$k_{2-}^2 = \frac{\chi_n - \chi_B}{2\chi_B - \chi_n}\left[1 + 2\sqrt{\chi_B(\chi_n - \chi_B)}\right],$$
$$\xi_{2-} = -\chi_B - \sqrt{\frac{\chi_B}{\chi_n - \chi_B}}. \tag{28}$$

Both the lower and the upper branches of instability boundary (in the sense of $|\xi|$ because $\xi < 0$ inside the instability region!) start at the point $\xi = \xi_\star^{(-)}$,

$$\xi_\star^{(-)} = \chi_B - \chi_n - \sqrt{\frac{\chi_B}{\chi_B - \chi_n}}.$$

At large $k \to \infty$, the function ξ on both branches asymptotically approaches the same value

$$\xi_\infty^{(-)} = -1 - \chi_B.$$

The lower branch approaches $\xi_\infty^{(-)}$ from above and the upper from below.

3. $\chi_n \leq \chi_B < \infty$

For this interval of χ_B only, the stationary point described by Eq. (18) is possible. As far as the necessary condition of instability requires that $\xi < -k^2\chi_B/(1+k^2)$, this stationary point is characterized by $\xi = \xi_{1-}$ and $k = k_{1-}$. It does exist for any $\chi_n > 0$ if $\chi_n \leq \chi_B < \chi_n + 1/2$. For such χ_B, the lower branch of instability boundary starting at the point $\xi = \xi_0$ at $k \to 0$ grows when k increases in the interval $0 < k < k_{1-}$ reaching its maximum corresponding to the critical value $\xi_{cr} = \xi_{1-}$ at $k = k_{1-}$. With further increase of k in the interval $k_{1-} < k < \infty$, the function ξ decreases and asymptotically approaches the value $\xi_\infty^{(-)} = -1 - \chi_B$. With the increase of χ_B the minimum of instability threshold $|\xi_{cr}|$ shifts from the modes with $k = 1/2\chi_n$ to the long-wavelength oscillations with $k = 0$.

For $\chi_n + 1/2 \leq \chi_B < \infty$, the function ξ on the branch of instability boundary $\sigma^2 = \mu_1$ is the decreasing function of k. It has the maximum at $k \to 0$ equal to ξ_0 which is the critical value of ξ and asymptotically approaches the value $\xi_\infty^{(-)}$ from above.

4. Summary

We have summarized the results of the above analysis in the form of several figures. In Fig. 2, the dependencies of the critical values of instability drive ξ_{cr} on χ_B for two fixed values of χ_n—$0 < \chi_n < 1$ and $\chi_n \geq 1$—are represented.

The dependencies of the wavenumbers and of the frequencies of marginally stable oscillations corresponding to ξ_{cr} are shown in Figs. 3 and 4.

One can see that for $0 < \chi_n < 1$ the long-wavelength oscillations require the minimal drive of instability if χ_B is either in the interval $\chi_B \in]-\infty, \chi_n - 1/2]$ or in the interval $\chi_B \in]\chi_n + 1/2, \infty[$. We show below that for such χ_n and χ_B and ξ which is close to ξ_{cr} only the long-wavelength low-frequency (compared to ω_{lh}) oscillations are unstable. For the other intervals of χ_B, the shorter-wavelength and higher-frequency modes have the minimal instability threshold.

For $\chi_n \geq 1$, the long-wavelength oscillations have the lowest threshold if either $\chi_B \in]-\infty, \chi_B^{(-)}]$, or $\chi_B \in]\chi_n - 1/2, \chi_B^{(+)}]$, or $\chi_B \in]\chi_n + 1/2, \infty[$. Otherwise, the shorter-wavelength and higher-frequency modes have the minimal instability threshold.

B. Frequencies and growth rates of unstable oscillations

We separately present the analysis of the frequencies and growth rates of unstable oscillations for the following ranges of χ_B: (a) $-\infty < \chi_B \leq \chi_n/2$ and $\chi_n \leq \chi_B < \infty$; (b) $\chi_n/2 < \chi_B < \chi_n$.

1. Unstable oscillations for $-\infty < \chi_B \leq \chi_n/2$ and $\chi_n \leq \chi_B < \infty$

As it follows from the above analysis of instability region, for equilibria with $0 < \chi_n < 1$ and $\chi_B \in]-\infty, \chi_n - 1/2]$ or $\chi_B \in]\chi_n + 1/2, \infty[$ and for equilibria with $\chi_n \geq 1$ and $\chi_B \in]-\infty, \chi_B^{(-)}]$ or $\chi_B \in [\chi_n + 1/2, \infty[$, the lower branch of instability boundary is the growing function of the oscillation wavenumber k. Then, assuming that the oscillations have the long wavelengths, $k^2 \equiv k_\perp^2 \rho_e^2 \ll 1$, and that the instability drive ξ

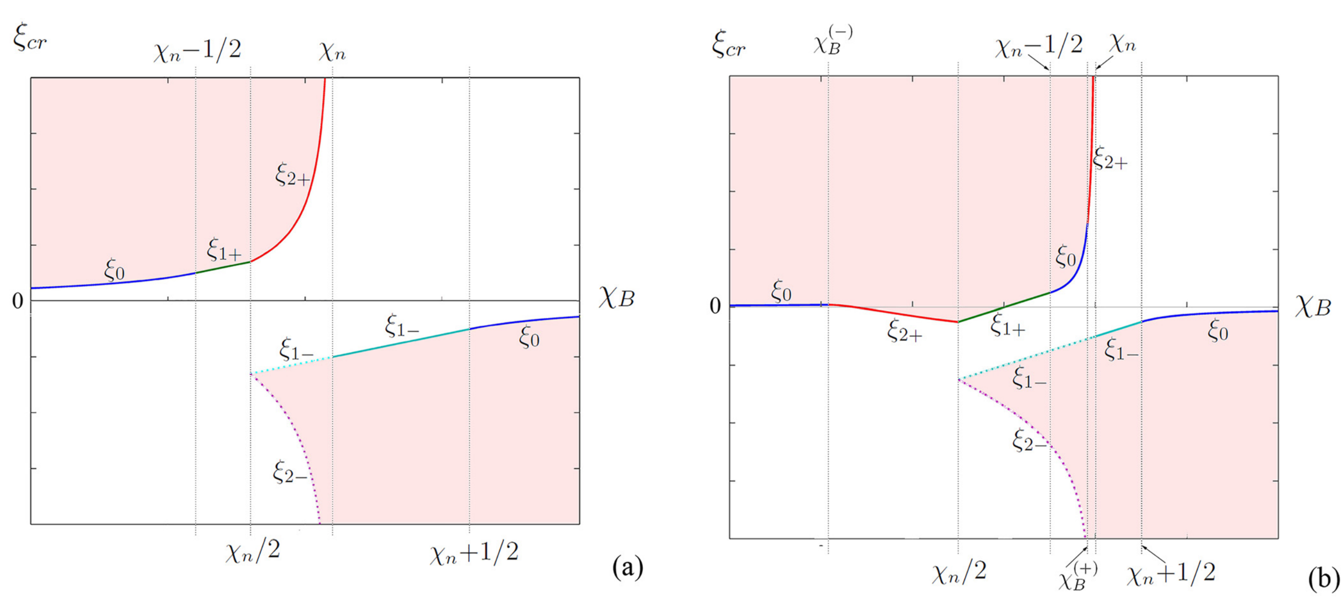

FIG. 2. Dependencies of critical values of instability drive, ξ_{cr}, on χ_B: (a) $\chi_n = 0.6$, (b) $\chi_n = 3$. Dashed lines show the upper and lower instability thresholds of short-wavelength oscillations with $k^2 > k_\star^2$ for $\chi_n/2 < \chi_B < \chi_n$.

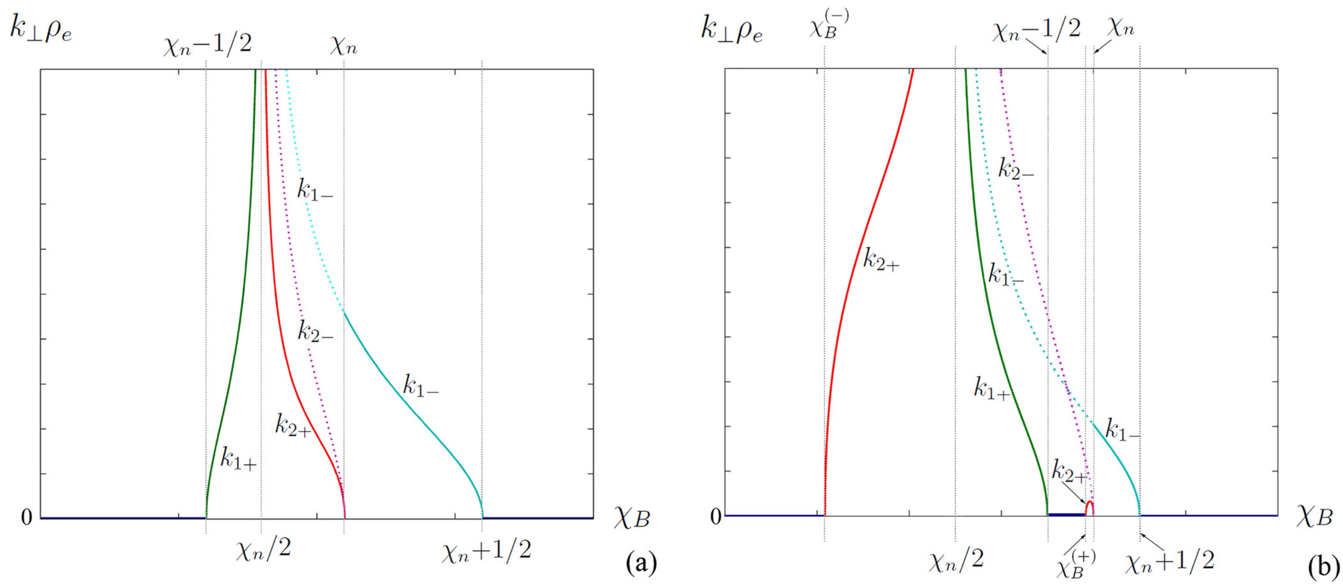

FIG. 3. Dependencies of wavenumbers, k, of marginally stable oscillations corresponding to ξ_{cr} on χ_B: (a) $\chi_n = 0.6$; (b) $\chi_n = 3$. Dashed lines show the wavenumbers of short-wavelength modes with $k^2 > k_\star^2$.

just slightly exceeds its critical value, $\xi = \xi_0\ (1 + O(k^2))$, we can show that the short-wavelength modes are stabilized by even small FLR effects.

Indeed, under the above assumptions, the following estimates are valid:

$$\frac{1}{\lambda\sigma} \sim k, \quad 4\lambda\sigma^2 + 1 - \frac{1}{2\lambda^2\sigma^2} \sim 1 - 4\xi(\chi_n - \chi_B) + O(k^2) \sim k^2.$$

Then, we simplify dispersion relation (6) and write it in the form

$$\bar{\Omega}^2 = \frac{1}{4\lambda^2\sigma^2}\left(4\lambda\sigma^2 + 1 - \frac{1}{2\lambda^2\sigma^2}\right) - \frac{3\bar{\Omega}}{4\lambda^3\sigma^3} - \frac{3\bar{\Omega}^2}{2\lambda^2\sigma^2} - \frac{\bar{\Omega}^3}{\lambda\sigma}, \quad (29)$$

where

$$\bar{\Omega} = \Omega - \frac{1}{2\lambda\sigma}. \quad (30)$$

It is evident that this equation is satisfied by $\bar{\Omega} \sim k^2$. Then keeping the terms up to order k^4 and neglecting the last three terms, we solve this equation and, returning to physical variables, obtain

$$\omega_r = \frac{k_\perp c_s^2}{2(V_{\star e} - V_D)} \cdot \mathrm{sgn}(k_y),$$
$$\gamma = \frac{k_\perp c_s^2}{2|V_{\star e} - V_D|} \cdot \sqrt{A_G - 1 - \alpha k_\perp^2 \rho_e^2}, \quad (31)$$

where ω_r and γ are the frequency and the growth rate of oscillations

$$A_G = 4\xi(\chi_n - \chi_B) \equiv -\frac{4(\kappa_n - 2\kappa_B)(V_{0E} + V_D)}{\omega_{Bi}},$$
$$\alpha = \left(1 - \frac{1}{4(\chi_n - \chi_B)^2}\right) \cdot (1 - 4\chi_B(\chi_n - \chi_B)). \quad (32)$$

The function A_G is proportional to the instability drive, and $A_G = 1$ corresponds to the critical value $\xi = \xi_{cr} \equiv \xi_0$. One can also check that for the values of χ_n and χ_B belonging to the assumed intervals the FLR effects are stabilizing, $\alpha > 0$. Therefore, the gradient-drift instability of considered long-wavelength oscillations is stabilized for the modes with $k_\perp \geq k_{\perp max}$, where

$$k_{\perp max}\,\rho_e = [(A_G - 1)/\alpha]^{1/2}.$$

The maximal growth rate among the unstable modes with $0 < k_\perp < k_{\perp max}$ belongs to the modes with $k_\perp\rho_e = [(A_G - 1)/2\alpha]^{1/2}$. The frequency and the growth rate of such oscillations are

$$\omega_r = \frac{c_s}{2(V_{\star e} - V_D)} \cdot \left(\frac{A_G - 1}{2\alpha}\right)^{1/2} \omega_{lh} \cdot \mathrm{sgn}(k_y),$$
$$\gamma = \frac{c_s \cdot (A_G - 1)}{4\alpha^{1/2}|V_{\star e} - V_D|} \cdot \omega_{lh}. \quad (33)$$

Such long-wavelength modes in neglect of the electron inertia and FLR effects have been studied previously, e.g., in Refs. 6 and 8. Such perturbation will be dominant only for plasma parameters near the critical value of the perpendicular current. Otherwise, as it can be shown below, there are always the high-frequency unstable oscillations with larger growth rates.

In the regions of equilibrium parameters where $0 < \chi_n < 1$, $\chi_B \in]-\infty, \chi_n - 1/2]$ and $\chi_n \geq 1$, $\chi_B \in]-\infty, \chi_B^{(-)}]$ with the increase of ξ, the spectrum of unstable modes gets wider and the maximum of instability growth rate shifts towards shorter wavelengths. At $\xi = 1 - \chi_B$, the whole spectrum of oscillations (up to $k^2 \to \infty$) is unstable. The similar picture takes place for $\chi_n > 0, \chi_B \in]\chi_n + 1/2, \infty[$. In this case, the instability takes place only for $\xi < 0$ and, therefore, when $-\xi$ grows, the spectrum of unstable modes gets wider and at $\xi = -1 - \chi_B$ the whole spectrum of oscillations becomes unstable.

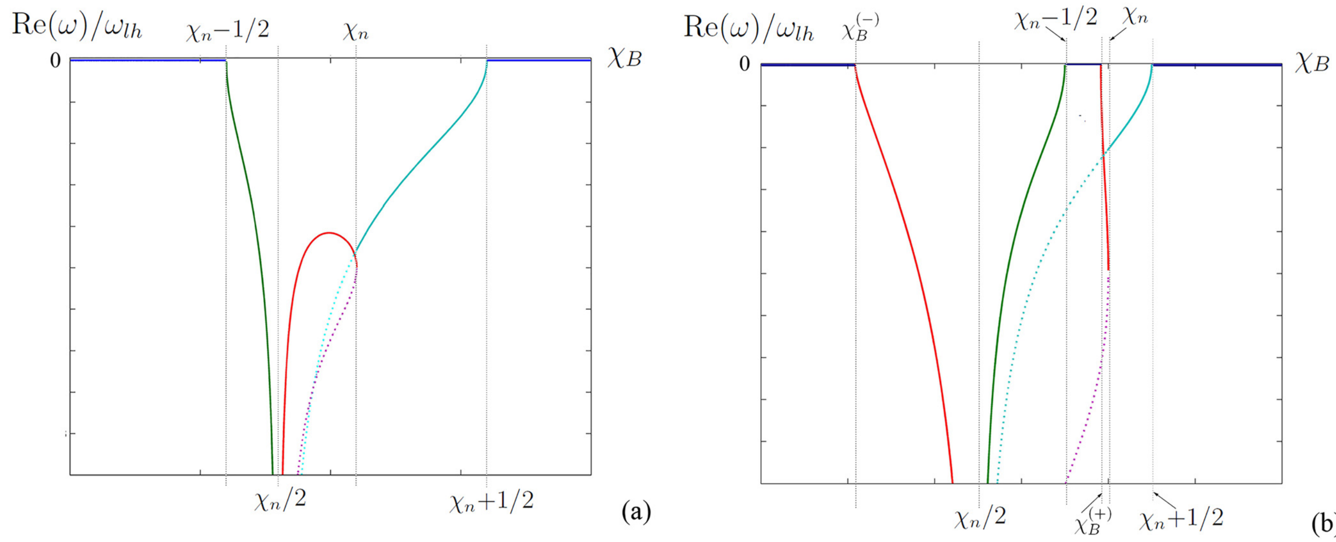

FIG. 4. Dependencies of frequencies ω of marginally stable oscillations corresponding to ξ_{cr} on χ_B: (a) $\chi_n = 0.6$, (b) $\chi_n = 3$. Dashed lines show the frequency of short-wavelength modes with $k^2 > k_\star^2$.

At $\xi = \pm 1 - \chi_B$ (in the corresponding region of parameters), the largest growth rate perturbations are the short-wavelength oscillations with $k \gg 1$. For such perturbations and the above mentioned values of ξ, we have $\sigma^2 \to 1$ and $\lambda \to 1$ and dispersion relation (6) is solved analytically. Namely, we rewrite this equation in the form

$$(\Omega + \sigma)^2(\Omega - \sigma) = \sigma(1-\lambda)\Omega^2 - (\sigma^2 - 1)(\Omega + \sigma). \quad (34)$$

Due to smallness of the right-hand side of this equation, its unstable solution can be represented in the form $\Omega = -\sigma + \delta\Omega$, where $\delta\Omega \sim k^{-1}$. Neglecting the last term on the right-hand side of Eq. (34), we find that $\delta\Omega$ satisfies the equation

$$2(\delta\Omega)^2 + \sigma^2(1-\lambda) = 0. \quad (35)$$

Solving this equation, we find that in physical variables the frequency and the growth rate of the most unstable modes with $k_\perp \rho_e \gg 1$ are as follows:

$$\omega_r \simeq k_\perp c_s \cdot \mathrm{sgn}\big(k_y(V_E + 2V_D)\big),$$
$$\gamma \simeq \omega_{lh} \cdot \left[\frac{1}{2}|\chi_n - 2\chi_B|\right]^{1/2}. \quad (36)$$

These oscillations can be identified as the high-frequency short-wavelength ion-sound waves. Also, it is important to notice that the growth rate of unstable oscillations saturates with the increase of $k_\perp$ and does not depend on $k_\perp$ when $k_\perp \to \infty$ [see Eq. (36)].

With a further increase of ξ, the spectrum of unstable modes narrows, and for large ξ, the electron inertia effects stabilize the oscillations with k^2 only slightly exceeding the value $k_0^2 = (\chi_n - \chi_B)/(\xi + \chi_B)$. The latter, $k = k_0$, is the solution of the equation $\lambda = 0$. The maximum of growth rate also shifts towards the long-wavelength high-frequency oscillations with $k^2 = k_0^2$. For

$$\frac{\chi_n - \chi_B}{\xi + \chi_B} \cdot (\xi + \chi_n - \chi_B) \gg 1,$$

the oscillations with largest growth rate are characterized by the following frequency and growth rate:

$$\omega_r = \frac{\omega_{lh}}{2} \cdot \left[\frac{\chi_n - \chi_B}{\xi + \chi_B} \cdot (\xi + \chi_n - \chi_B)^2\right]^{1/6} \cdot \mathrm{sgn}\big(k_y(V_E + V_{\star e})\big),$$
$$\gamma = \frac{\sqrt{3}\,\omega_{lh}}{2} \cdot \left[\frac{\chi_n - \chi_B}{\xi + \chi_B} \cdot (\xi + \chi_n - \chi_B)^2\right]^{1/6}. \quad (37)$$

In the limiting case $\xi \gg (\chi_n, \chi_B)$, expressions (37) are simplified and we get (compare with Refs. 19 and 20)

$$\omega_r = \frac{\omega_{lh}}{2} \cdot [\xi(\chi_n - \chi_B)]^{1/6} \cdot \mathrm{sgn}\big(k_y(V_E + V_{\star e})\big),$$
$$\gamma = \frac{\sqrt{3}\,\omega_{lh}}{2} \cdot [\xi(\chi_n - \chi_B)]^{1/6}. \quad (38)$$

Such oscillations have long wavelengths, $k_\perp \rho_e \simeq ((\chi_n - \chi_B)/\xi) \ll 1$.

The contour-plots of the growth rates and frequencies of unstable modes for the discussed ranges of parameters χ_n and χ_B calculated from dispersion relation (6) using the trigonometrical Vieta's formula in the plane $k_\perp - \xi$ are presented in Fig. 5 for $\chi_n = 6$ and $\chi_B = -6$.

Also, Fig. 6 shows the dependencies of the growth rates and frequencies of unstable perturbations for $\chi_n = 6$, $\chi_B = -6$ and different values of ξ.

In the regions with $0 < \chi_n < 1$ and $\chi_B \in]\chi_n - 1/2, \chi_n/2]$, the instability threshold starts at $\xi = \xi_0$ when $k^2 \to 0$ and then decreases with the increase of k^2 up to $k^2 = k_{1+}^2$ reaching the minimal value ξ_{1+}. It means that for $\xi_{1+} < \xi < \xi_0$ the long-wavelength perturbations are stable. The instability starts from some minimal k^2 which is the root of equation $\sigma^2 = \mu_1$. The minimal threshold corresponds to the high-frequency waves with ω_r of order ω_{lh}. Due to the FLR effects, the short-wavelength modes are stabilized when k^2 reaches some maximal wavenumber.

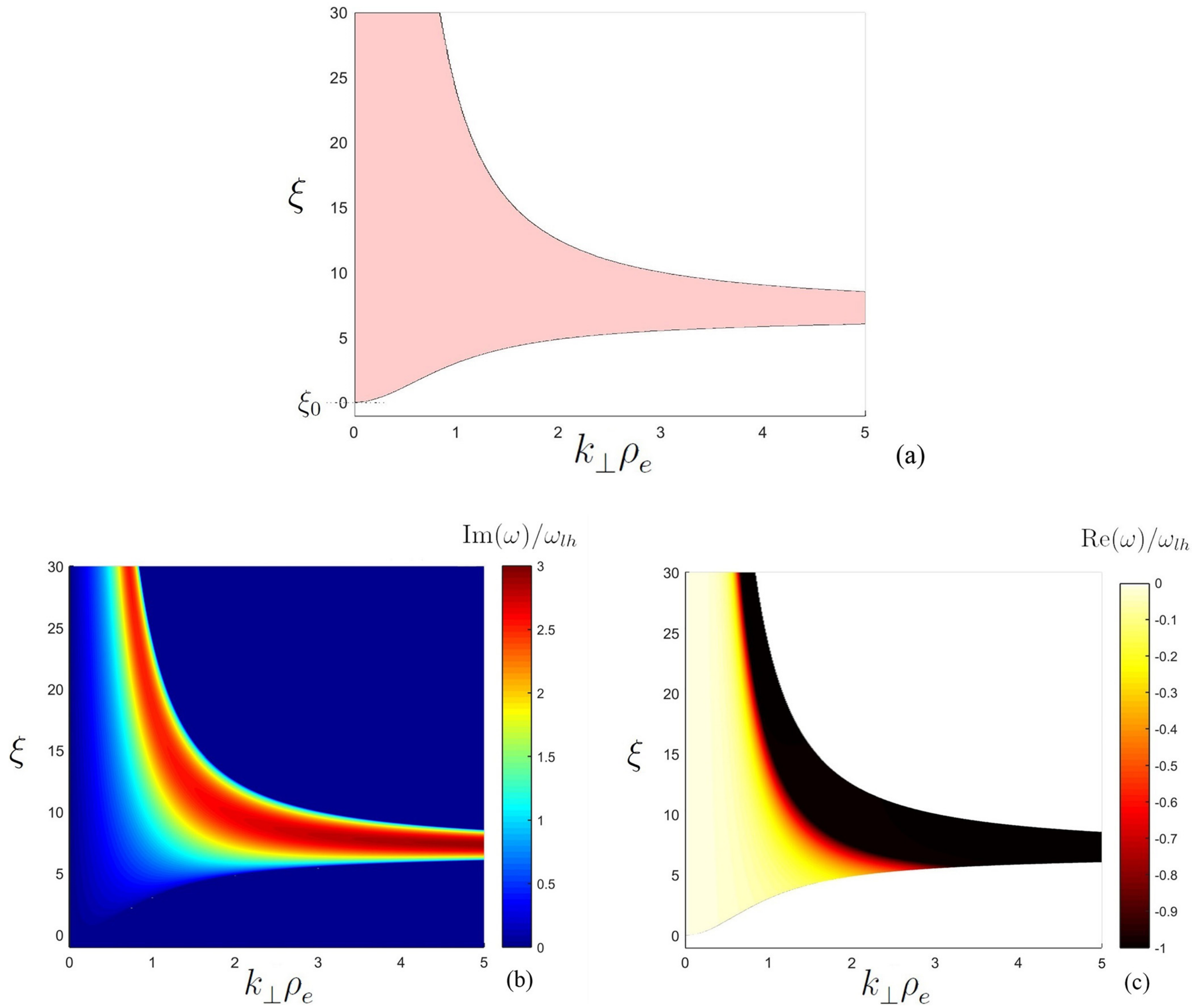

FIG. 5. Stability diagram in (k, ξ)-plane (the instability region is shaded) (a); contour-plots of the growth rates (b) and frequencies (c) of unstable modes in $k_\perp - \xi$-plane. Here, $\chi_n = 6, \chi_B = -6$. In Fig. 5(c), the white color indicates the stable region and oscillations with frequency higher than ω_{lh} are shown in black.

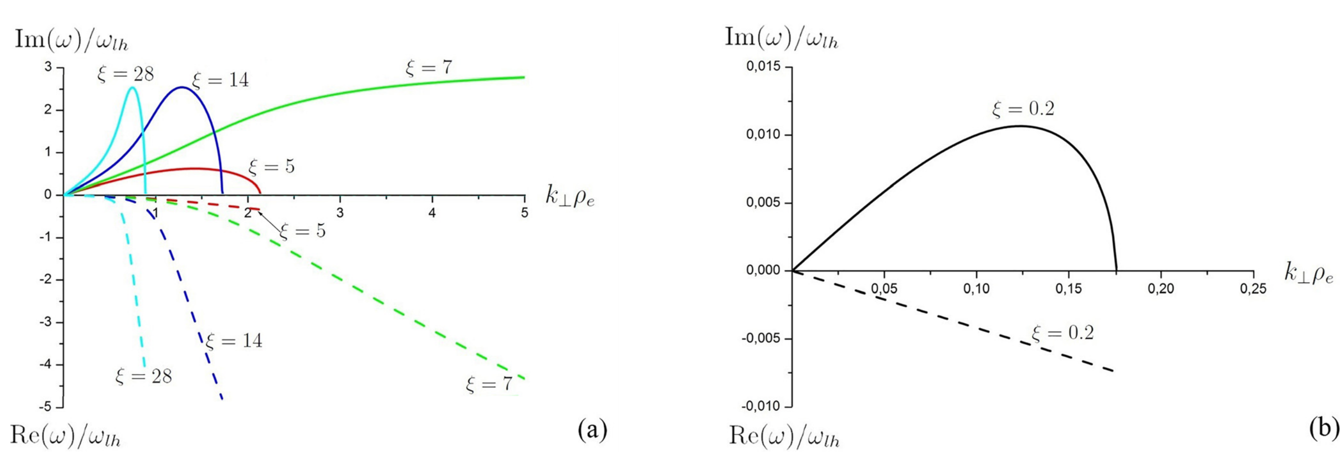

FIG. 6. Dependencies of growth rates and frequencies of unstable modes on wavenumber $k_\perp$ (a); the near-threshold region is shown separately in Fig. 6(b). Different lines correspond to different values of ξ. Here $\chi_n = 6, \chi_B = -6$.

For

$$\chi_n - 1/2 < \chi_B \le \frac{1}{2}\left(1 + \chi_n - \sqrt{1 + (1 - \chi_n)^2}\right),$$

this maximal wavenumber is another larger root of equation $\sigma^2 = \mu_1$. The growth rate increases with the increase of ξ in the interval $\xi_{1+} < \xi < \xi_0$ and the instability region expands both into the larger- and shorter-wavelength domains.

For

$$\frac{1}{2}\left(1 + \chi_n - \sqrt{1 + (1 - \chi_n)^2}\right) < \chi_B < \frac{\chi_n}{2},$$

the wavenumber of the shortest unstable oscillations is as follows: (1) another larger root of equation $\sigma^2 = \mu_1$ if $\xi < 1 - \chi_B$; (2) the root of equation $\sigma^2 = \mu_2$ (the point of intersection of the curve σ^2 with the upper branch of instability threshold) if $\xi > 1 - \chi_B$. For $\xi = 1 - \chi_B$, the whole spectrum of oscillations is unstable. The largest growth rate perturbations are the high-frequency ion-sound waves described by Eq. (36). The spectrum of unstable modes expands in the long-wavelength region up to $k \to 0$ when $\xi > \xi_0$. Like it is described above for another interval of parameters χ_n and χ_B, further increase of ξ in the interval $\xi > 1 - \chi_B$ results in narrowing of instability spectrum and stabilization of short-wavelength modes for $\xi \gg 1$ at k of order k_0. The oscillations with $k \simeq k_0$ have the maximal growth rate and are characterized by Eq. (38).

The contour-plots of the growth rates and frequencies of unstable modes for the discussed ranges of parameters χ_n and χ_B in the plane $k_\perp - \xi$ are presented in Fig. 7 for $\chi_n = 0.5$ and $\chi_B = 0.15$.

Also, Fig. 8 shows the dependencies of the growth rates and frequencies of unstable perturbations for $\chi_n = 0.5, \chi_B = 0.15$ and different values of ξ.

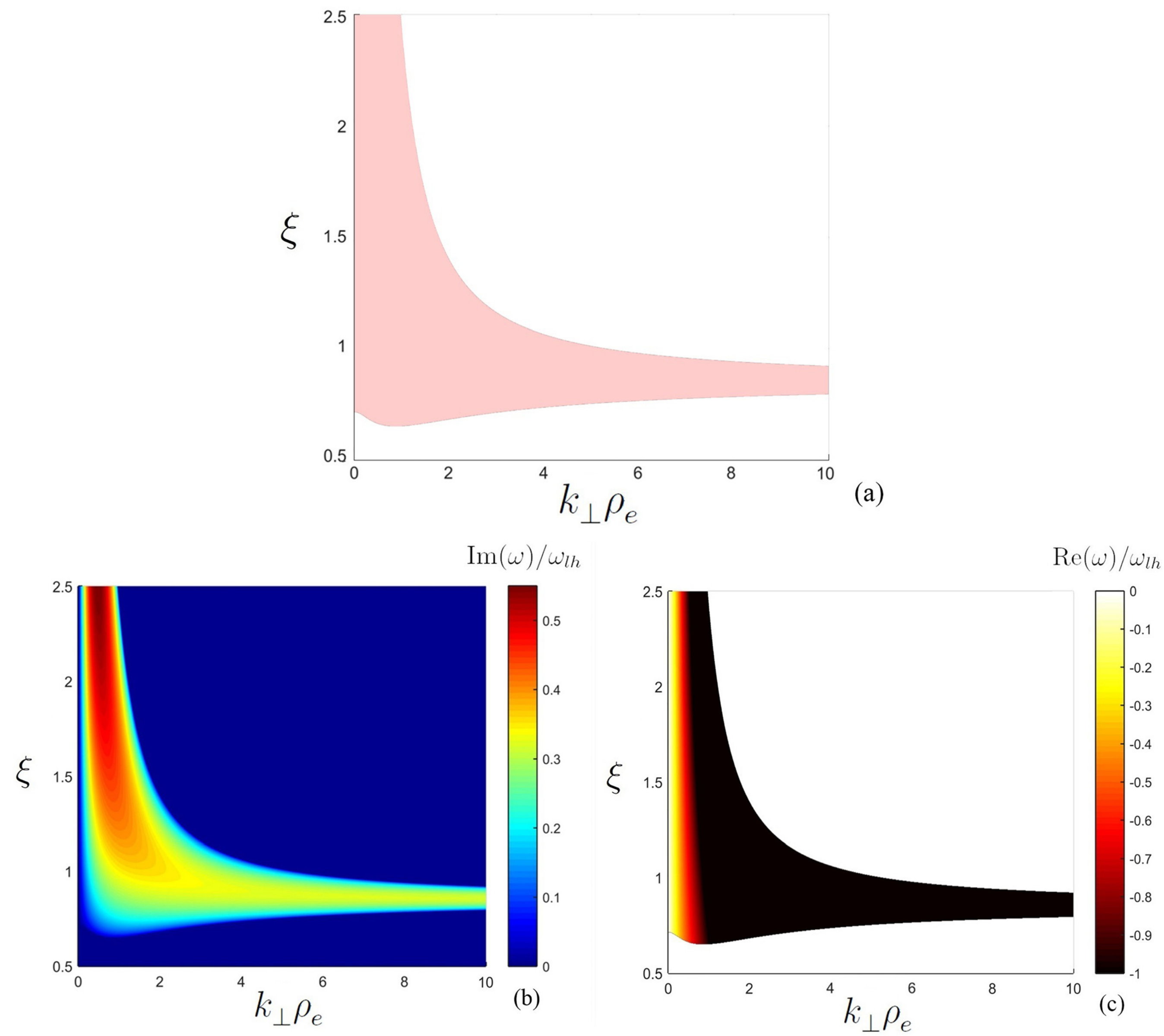

FIG. 7. Stability diagram in (k, ξ)-plane (the instability region is shaded) (a); contour-plots of the growth rates (b) and frequencies (c) of unstable modes in $k_\perp - \xi$-plane. Here $\chi_n = 0.5, \chi_B = 0.15$. In Fig. 7(c), the white color indicates the stable region and oscillations with frequency higher than ω_{lh} are shown in black.

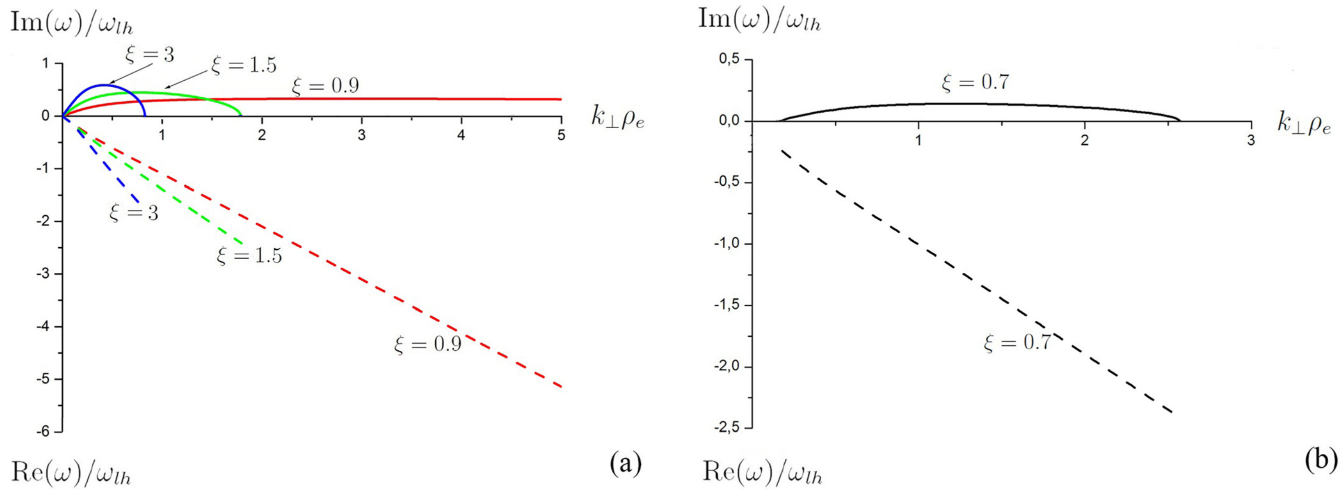

FIG. 8. Dependencies of growth rates and frequencies of unstable modes on wavenumber $k_\perp$ (a); the near-threshold region is shown separately in Fig. 8(b). Different lines correspond to different values of ξ. Here, $\chi_n = 0.5, \chi_B = 0.15$.

A similar behavior of the frequencies and growth rates of unstable oscillations takes place in the regions where $\chi_n \geq 1$, $\chi_B \in]\chi_B^{(-)}, \chi_n/2]$ (with the substitution $\xi_{1+} \to \xi_{2+}, k_{1+} \to k_{2+}$) and where $\chi_n > 0, \chi_B \in [\chi_n, \chi_n + 1/2[$ (with the substitution $\xi_{1+} \to \xi_{1-}, k_{1+} \to k_{1-}$). In the latter case, the necessary condition of instability is $\xi < 0$ and the lower branch of instability threshold has its maximum ξ_{1-}. So, the growth rate of instability increases when ξ decreases, i.e., when $-\xi$ increases.

2. Unstable oscillations for $\chi_n/2 < \chi_B < \chi_n$

In accordance with the analysis of Subsection III A in the regions with $0 < \chi_n < 1$, the gradient drift instability occurs either when the drive ξ is positive and $\xi > \xi_{2+}$ or when it is negative and $\xi_{2-} < \xi < \xi_{1-}$ (see Fig. 9). In the former case, the long-wavelength oscillations with $k^2 < k_\star^2$ can be unstable, and in the latter, only the short-wavelength oscillations which always have high-frequencies can be unstable.

For positive drive in the interval $\xi_{2+} < \xi < \xi_0$, the instability starts from some minimal finite value of $k \neq 0$ which is the root of equation $\sigma^2 = \mu_1$. This means that for such drives the long-wavelength oscillations are stable. The closer the ξ to ξ_0, the longer-wavelength oscillations are unstable. The electron inertia and FLR effects also stabilize the short-wavelength modes. Thus, the instability takes place for $k_{min} < k < k_{max}$. The results of numerical analysis show that high-frequency modes with $\omega \sim \omega_{lh}$ have the largest growth rate (see Fig. 10). For $\xi > \xi_0$, the long-wavelength oscillations with $k \to 0$ become unstable and the short-wavelength oscillations are stabilized at some $k = k_{max}$. With the increase of ξ, the spectrum of unstable perturbations narrows and the maximum of the growth rate shifts towards $k = k_0$. Such oscillations are described by expressions (37) and (38).

For negative drive such that $\xi_{2-} < \xi < \xi_{1-}$ the unstable oscillations have high frequencies of order ω_{lh} and higher. Also, we notice that for $\xi = -1 - \chi_B$ the oscillations with k up to $k \to \infty$ are unstable. The largest growth rate perturbations are the high-frequency ion-sound waves characterized by expressions (36).

The dependencies of the growth rates and frequencies of unstable perturbations on wavenumber $k_\perp$ for $\chi_n = 0.5, \chi_B = 0.4$ and different values of ξ are represented in Fig. 11.

Qualitatively the same picture for the instability region, the growth rate, and frequencies remains for $\chi_n \geq 1$. The difference is that in this case the critical instability drive for the perturbations with $k < k_\star$ depends on the value of χ_B. For $\chi_B \in]\chi_n/2, \chi_n - 1/2[$, the instability occurs at $\xi > \xi_{1+}$, for $\chi_B \in]\chi_B^{(+)}, \chi_n[$—at $\xi > \xi_{2+}$, and for $\chi_B \in [\chi_n - 1/2, \chi_B^{(+)}]$—at $\xi > \xi_0$. In the latter case, there is no cutoff of instability at long wavelengths and it starts from the longest-wavelength oscillations with $k \to 0$.

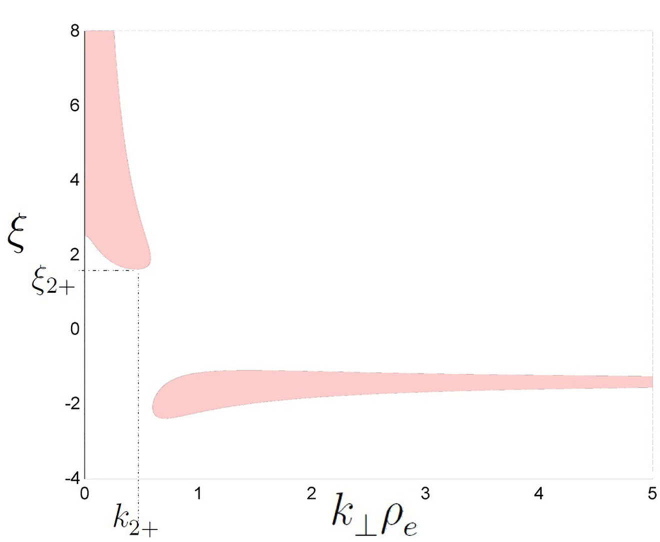

FIG. 9. Stability diagram in (k, ξ)-plane for $\chi_n = 0.5$, $\chi_B = 0.4$. The instability regions are shaded.

IV. INSTABILITY DRIVEN BY THE ELECTRON MAGNETIC DRIFT

Now, let us analyze a stability of azimuthal oscillations in the regions of negligibly weak electric field, such that $|eE_0/(\kappa_B T_e)| \ll 1$. Neglecting the effects of equilibrium

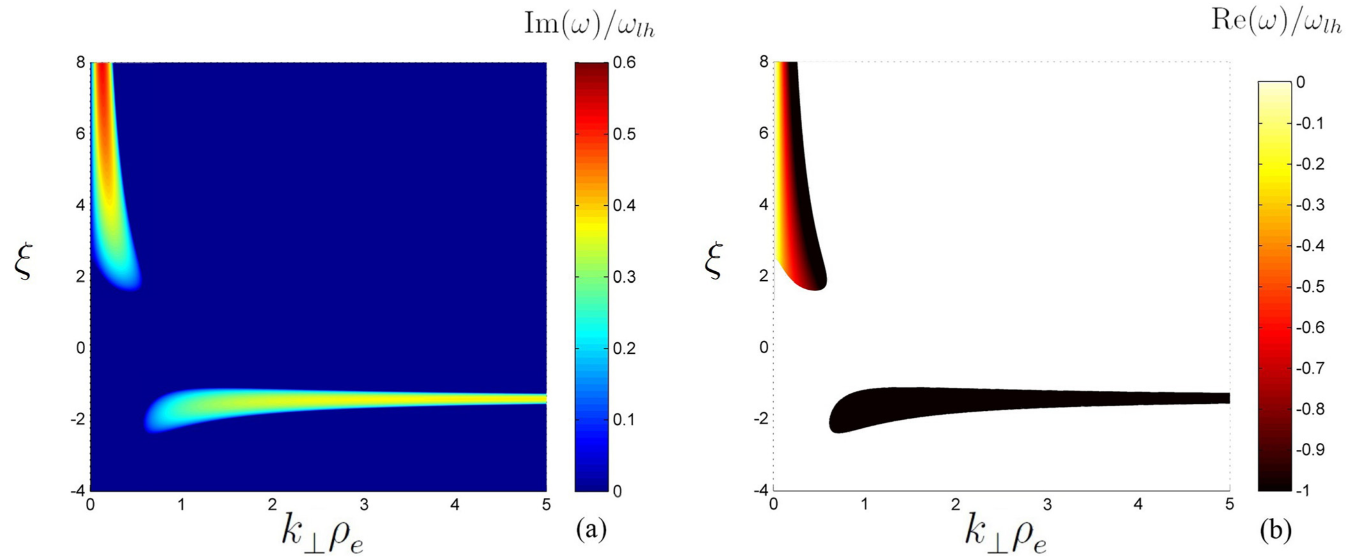

FIG. 10. Contour-plots of the growth rates (a) and frequencies (b) of unstable modes in $k_\perp - \xi$-plane. Here, $\chi_n = 0.5, \chi_B = 0.4$. In Fig. 10(b), the white color indicates stable region, and oscillations with frequency higher than ω_{lh} are shown in black.

electric field, we find that the coefficients in dispersion relation (6) take the form

$$\lambda = 1 - \frac{(1+k^2)\chi_n - (1+2k^2)\chi_B}{k^2(1+2k^2)\chi_B},$$
$$\sigma = \frac{k(1+2k^2)\,\mathrm{sgn}(k_y)}{(1+k^2)^{3/2}} \cdot \chi_B. \tag{39}$$

The perturbations are characterized only by two independent parameters χ_n and χ_B. As we have already shown earlier, the gradient drift instability is due to a combination of equilibrium electron drift (instability drive) and inhomogeneity of plasma and magnetic field in the direction perpendicular to the magnetic field (instability trigger). It is important to notice that in the regions of negligibly weak electric field one of the parameters, χ_B, enters the dispersion relation in two ways. On the one hand, the instability is driven by the electron magnetic drift, which is proportional to the magnetic field inhomogeneity and characterized by the parameter χ_B, as the drive χ_B enters the dispersion relation via the coefficient σ and via the denominator in the expression of λ. On the other hand, the magnetic field gradient in combination with the plasma density gradient enters the inhomogeneity term (the numerator in the expression of λ) serving as a trigger of instability. Due to this intrinsic coupling between the instability drive and its trigger in a finite electron temperature plasmas, this problem is in some sense degenerate and needs to be treated separately. We show that this specifics results in severe restriction of instability domain.

Let us notice again that the coefficients λ and σ do not change under the substitution $\chi_n \to -\chi_n$, $\chi_B \to -\chi_B$, $k_y \to -k_y$. Therefore, hereafter we fix $\chi_n > 0$ and study the instability picture changing its drive V_D, i.e., the value of χ_B.

A. Marginal stability condition and instability region

The necessary condition for the instability $\lambda < 1$ in the considered case takes the form

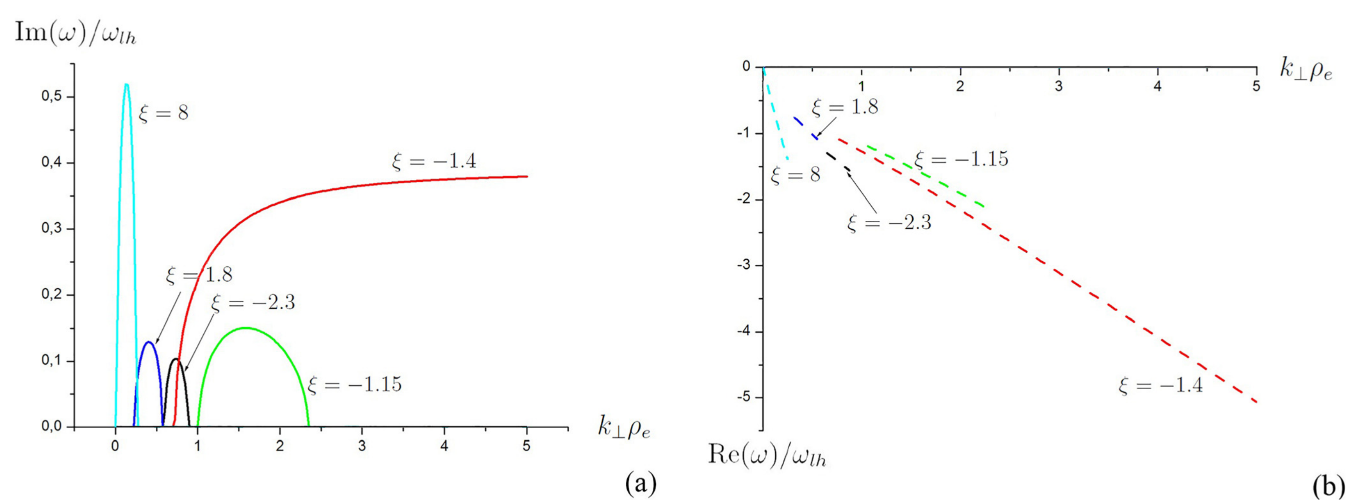

FIG. 11. Dependencies of growth rates (a) and frequencies (b) of unstable modes on wavenumber $k_\perp$. Different lines correspond to different values of ξ. Here, $\chi_n = 0.5, \chi_B = 0.4$.

$$0 < \chi_B < \chi_n,$$

and the instability domain is described by the inequalities (see also Ref. 14),

$$\begin{cases} \chi_B^2 > \mu_1 f(k), & \text{for } k^2 \le (\chi_n - \chi_B)/2\chi_B; \\ \mu_1 f(k) < \chi_B^2 < \mu_2 f(k), & \text{for } k^2 > (\chi_n - \chi_B)/2\chi_B, \end{cases} \tag{40}$$

where

$$f(k) = \frac{(1+k^2)^3}{k^2(1+2k^2)^2}. \tag{41}$$

The instability is driven by the equilibrium electron magnetic drift. It arises only when the electron magnetic drift velocity V_D exceeds some minimal value, i.e., when $\chi_B > (\chi_B)_{min}$. At the same time, the inhomogeneity defined by the parameter $\chi_n - \chi_B$ decreases when the drive χ_B increases and goes to zero at $\chi_B \to \chi_n$. Thus, the instability is possible only when $(\chi_B)_{min} < \chi_B < (\chi_B)_{max}$. To better understand this point, let us start from the long-wavelength perturbations with $k \to 0$. Expanding the functions $\lambda, \mu_{1,2}$ and f in a power series over k for $k \ll 1$, we find that for such perturbations the instability condition $\chi_B^2 > \mu_1 f(k)$ takes the form

$$\chi_B \cdot (\chi_n - \chi_B) > \frac{1}{4}\left[1 + \left(\frac{\chi_n - 2\chi_B}{\chi_n - \chi_B}\right)^2 k^4 + O(k^6)\right]. \tag{42}$$

Thus, for $k \to 0$, the gradient drift instability is possible only if

$$\frac{1}{2}\left(\chi_n - \sqrt{\chi_n^2 - 1}\right) < \chi_B < \frac{1}{2}\left(\chi_n + \sqrt{\chi_n^2 - 1}\right), \ \ \chi_n^2 > 1. \tag{43}$$

The terms of order k^4 in Eq. (42) demonstrate that the lower boundary of instability $(\chi_B)_{min}$ increases with the growth of k and the upper boundary $(\chi_B)_{max}$ decreases. Thus, the region of instability for long-wavelength perturbations, $k \ll 1$, gets narrower with respect to χ_B when k increases.

To prove that for any $0 < k < \infty$, the minimal and maximal values of χ_B are described by the corresponding expressions in inequality (43), we turn to Eq. (14) describing the instability boundary. We consider it as the equation defining the implicit function $\chi_B = \chi_B(k)$ at fixed χ_n and look for its extremums in the interval $0 < k < \infty$. A lengthy but straightforward analysis shows that there are no solutions of Eq. (17) describing the stationary points. Therefore, the function χ_B has no stationary points. It means that the extremes of χ_B take place at the edge points $k = 0$ and $k = \infty$. We have already found the minimal and maximal values of χ_B at $k = 0$. When $k \to \infty$, we have $\lambda \to 1$, $\mu_{1,2} \to 1$ and both the lower and the upper instability boundaries asymptotically approach the same value—$\chi_B = 1/2$. Thus, at fixed χ_n, the instability takes place only at $|V_{\star e}| > c_s$. It starts when the electron magnetic drift velocity $|V_D|$ exceeds the lower critical value $V_{cr}^{(-)}$,

$$V_{cr}^{(-)} = \frac{1}{2}\left(|V_{\star e}| - \sqrt{V_{\star e}^2 - c_s^2}\right), \tag{44}$$

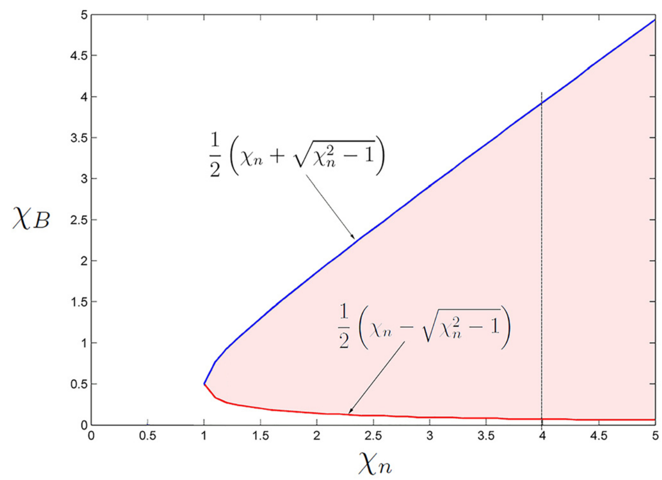

FIG. 12. Stability diagram in the plane χ_n–χ_B. The instability region is shaded.

and stops when $|V_D|$ reaches the upper critical value $V_{cr}^{(+)}$,

$$V_{cr}^{(+)} = \frac{1}{2}\left(|V_{\star e}| + \sqrt{V_{\star e}^2 - c_s^2}\right). \tag{45}$$

The instability region in the plane χ_n–χ_B is presented in Fig. 12.

The instability region in the plane χ_B–$k_\perp$ is presented in Fig. 13. For $|\chi_B| = 1/2$, the whole spectrum of perturbations $0 < k < \infty$ is unstable. For $|\chi_B| < 1/2$, the value of $(k_\perp)_{max} = k_\star$ at which the electron FLR effects stabilize the gradient drift instability is defined by equation $\chi_B^2 = \mu_1(k_\star)f(k_\star)$ and for $|\chi_B| > 1/2$ by equation $\chi_B^2 = \mu_2(k_\star)f(k_\star)$. The value of $k_\star$ increases and the spectrum of unstable perturbations expands when $|V_D|$ increases from $V_{cr}^{(-)}$ to $c_s/2$ and narrows when $|V_D|$ further increases from $c_s/2$ to $V_{cr}^{(+)}$.

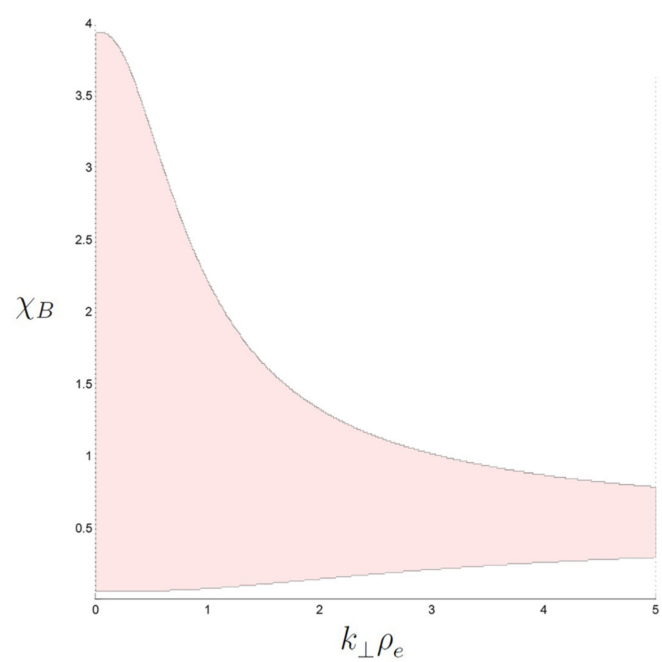

FIG. 13. Stability diagram in the plane χ_B–$k_\perp$ for $\chi_n = 4$. The instability region is shaded.

B. Frequencies and growth rates of oscillations driven by electron magnetic drift

The above analysis of instability domain presented by Fig. 13 shows that for the values of electron magnetic drift velocity $|V_D|$ near the lower, $V_{cr}^{(-)}$, and upper, $V_{cr}^{(+)}$, critical values, only the long-wavelength perturbations are unstable and shorter-wavelength modes are stabilized by the electron FLR effects. In this limiting case, it is possible to solve dispersion relation (6) analytically by assuming that $|V_D| - V_{cr}^{(-)}$ (or $V_{cr}^{(+)} - |V_D|$) is as small as k^4 and applying the expansion of the eigenfrequency Ω and dimensionless coefficients λ and σ in powers of k.

To do that, we rewrite Eq. (6) in the form described by Eqs. (29) and (30). Then, using expressions (39), we obtain the following estimates:

$$\frac{1}{\lambda\sigma} \sim k,\ 4\lambda\sigma^2 + 1 - \frac{1}{2\lambda^2\sigma^2} \sim k^4.$$

Thus, Eq. (6) can be satisfied if we assume that $\bar{\Omega} \sim k^3$. Under this assumption, it can be simplified by neglecting the last two terms on the right-hand side and written in the form

$$\left(\bar{\Omega} + \frac{3}{8\lambda^3\sigma^3}\right)^2 = \frac{1}{4\lambda^2\sigma^2}\left(4\lambda\sigma^2 + 1 - \frac{1}{2\lambda^2\sigma^2} + \frac{9}{16\lambda^4\sigma^4}\right).$$

Unlike the general case analyzed above here, the FLR corrections to the mode eigenfrequency are of higher order with respect to small parameter k and more terms need to be taken into account. Representing Ω in the form $\Omega = \Omega_r + i\Gamma$, where Ω_r is the normalized mode frequency and Γ is its normalized growth rate, we obtain

$$\Omega_r = \frac{1}{2\lambda\sigma}\left(1 + O(k^2)\right),$$
$$\Gamma = \frac{1}{2|\lambda\sigma|}\left[-4\lambda\sigma^2 - 1 + \frac{1}{2\lambda^2\sigma^2} - \frac{9}{16\lambda^4\sigma^4}\right]^{1/2}.$$

Finally, substituting here expressions (39) and remembering the definitions of Ω and k [see Eq. (7)], we arrive at the following result:

$$\omega_r \simeq \frac{k_\perp c_s^2 \cdot \mathrm{sgn}(k_y)}{2(V_{\star e} - V_D)},$$
$$\gamma = \frac{k_\perp c_s^2}{|V_{\star e} - V_D|} \cdot \left[\chi_B(\chi_n - \chi_B) - \frac{1}{4} - \frac{1}{4}\left(\frac{\chi_n - 2\chi_B}{\chi_n - \chi_B}\right)^2 \cdot k_\perp^4\rho_e^4\right]^{1/2}. \tag{46}$$

Then, for $|V_D|$ near the lower critical value $V_{cr}^{(-)}$, we obtain the low-frequency long-wavelength mode with the frequency and the growth rate described by

$$\omega_r^{(l)} \simeq \frac{k_\perp c_s^2}{|V_{\star e}| + \sqrt{V_{\star e}^2 - c_s^2}} \cdot \mathrm{sgn}(k_y V_{\star e}),$$
$$\gamma^{(l)} = \frac{2k_\perp c_s (V_{\star e}^2 - c_s^2)^{1/4}}{|V_{\star e}| + \sqrt{V_{\star e}^2 - c_s^2}} \times \left[|V_D| - V_{cr}^{(-)} - \frac{c_s^2\sqrt{V_{\star e}^2 - c_s^2} \cdot k_\perp^4\rho_e^4}{\left(|V_{\star e}| + \sqrt{V_{\star e}^2 - c_s^2}\right)^2}\right]^{1/2}. \tag{47}$$

The gradient drift instability takes place for $|V_D| > V_{cr}^{(-)}$ and only for the perturbations with

$$k_\perp^4\rho_e^4 < \frac{\left(|V_{\star e}| + \sqrt{V_{\star e}^2 - c_s^2}\right)^2\left(|V_D| - V_{cr}^{(-)}\right)}{c_s^2\sqrt{V_{\star e}^2 - c_s^2}} \equiv k_-^4\rho_e^4. \tag{48}$$

The growth rate has its maximum for the oscillations with $(k_\perp)_{max}^{(-)} = k_-/3^{1/4}$. The frequency and the growth rate of the most unstable mode are

$$(\omega_r)_{max}^{(l)} \simeq \left[\frac{1}{3} \cdot \frac{c_s^2\left(|V_D| - V_{cr}^{(-)}\right)}{\sqrt{V_{\star e}^2 - c_s^2}\left(|V_{\star e}| + \sqrt{V_{\star e}^2 - c_s^2}\right)^2}\right]^{1/4} \times \omega_{lh} \cdot \mathrm{sgn}(k_y V_{\star e}),$$
$$(\gamma)_{max}^{(l)} = \left[\frac{8}{3} \cdot \frac{\sqrt{V_{\star e}^2 - c_s^2}\left(|V_D| - V_{cr}^{(-)}\right)}{c_s^2}\right]^{1/2} \times |(\omega_r)_{max}^{l}| \ll |(\omega_r)_{max}^{l}|. \tag{49}$$

The frequency $\omega_r^{(h)}$ and growth rate $\gamma_r^{(h)}$ of oscillations in the region, where $|V_D|$ is close to the upper instability boundary $V_{cr}^{(+)}$, are described by the equations which follow from Eq. (47) by the substitutions

$$\omega_r^{(l)} \to \omega_r^{(h)},\ \gamma_r^{(l)} \to \gamma_r^{(h)},\ |V_{\star e}| + \sqrt{V_{\star e}^2 - c_s^2} \to |V_{\star e}| - \sqrt{V_{\star e}^2 - c_s^2},\ |V_D| - V_{cr}^{(-)} \to V_{cr}^{(+)} - |V_D|.$$

In a similar way, the wavenumber k_+ at which the stabilization of instability by the FLR effects takes place, the wavenumber, frequency $(\omega_r)_{max}^{(h)}$ and growth rate $(\gamma)_{max}^{(h)}$ of the perturbation with the largest growth rate are described by expressions (48) and (49) with the additional substitutions

$$k_- \to k_+,\ (\omega_r)_{max}^{(l)} \to (\omega_r)_{max}^{(h)},\ (\gamma)_{max}^{(l)} \to (\gamma)_{max}^{(h)}.$$

For fixed $V_{\star e}$ with the increase of the magnetic drift velocity in the interval between the lower critical value $V_{cr}^{(-)}$ and $2c_s$, $V_{cr}^{(-)} < |V_D| < 2c_s$, the spectrum of unstable perturbations expands into the region of short-wavelengths. The maximal growth rate of instability increases. It takes place for the oscillations with shorter and shorter wavelengths and the frequency of oscillations with the maximal growth rate also increases.

For $|V_D| = 2c_s$ (or $|\chi_B| = 1/2$), the whole spectrum of oscillations (up to $k_\perp\rho_e \to \infty$) is unstable. In this case, the frequency of unstable oscillations increases with the increase of $k_\perp$ and the growth rate also increases and has its maximum at large $k_\perp \rho_e \to \infty$. For perturbations with $k \gg 1$,

$$\lambda = 1 - \frac{|\chi_n| - 1}{k^2} + O\left(\frac{1}{k^4}\right),$$
$$\sigma = \left[1 - \frac{1}{k^2} + O\left(\frac{1}{k^4}\right)\right] \cdot \mathrm{sgn}(k_y), \tag{50}$$

so that $(\lambda, \sigma^2) \to 1$ when $k \to \infty$. Then, dispersion relation (6) can be solved analytically similarly to Sec. II [see Eqs. (33)–(35)]. As a result, we find that in physical variables, the frequency and the growth rate of the most unstable modes with $k_\perp \rho_e \gg 1$ are as follows:

$$\omega_r \simeq k_\perp c_s \cdot \mathrm{sgn}(k_y V_D) \equiv 2k_\perp V_D \cdot \mathrm{sgn}(k_y),$$
$$\gamma \simeq \omega_{lh} \cdot \left(\frac{|\chi_n| - 1}{2}\right)^{1/2} \equiv \omega_{lh} \cdot \left[\frac{1}{2}\left(\frac{|V_{\star e}|}{c_s} - 1\right)\right]^{1/2}. \tag{51}$$

These perturbations can be identified as the high-frequency ion-sound waves.

When $|V_D|$ increases further in the interval $2c_s < |V_D| < V_{cr}^{(+)}$, the spectrum of unstable oscillations gets narrower. The short-wavelength modes are stabilized due to electron inertia and FLR effects. For $|V_D|$ not too close to $V_{cr}^{(+)}$, such that $(V_{cr}^{(+)} - V_D)/V_{cr}^{(+)} \sim 1$, the maximal growth rate belongs to the oscillations with $k_\perp^2 \rho_e^2 \simeq (V_{\star e} - V_D)/2V_D$. For such perturbations $\lambda \simeq 0$, and the dispersion relation reduces to $\Omega^3 - \Omega - \sigma = 0$.

If, in addition, $|V_{\star e}| \gg c_s$, so that $\sigma^2 \gg 1$, the maximal growth rate and the frequency corresponding to it are described by

$$\omega_r = \frac{\omega_{lh}}{2} \cdot \left[-\frac{V_{\star e}^2}{2V_D^2}\frac{(\kappa_n - 2\kappa_B)V_D}{\omega_{Bi}}\right]^{1/6} \cdot \mathrm{sgn}(k_y V_D),$$
$$\gamma = \frac{\sqrt{3}\,\omega_{lh}}{2} \cdot \left[-\frac{V_{\star e}^2}{2V_D^2}\frac{(\kappa_n - 2\kappa_B)V_D}{\omega_{Bi}}\right]^{1/6}. \tag{52}$$

In Figs. 14(a) and 14(b), the contour-plots of the growth rates and frequencies of unstable modes calculated using the trigonometrical Vieta's formula in the plane $k_\perp - \chi_B$ are shown for $\chi_n = 4$. Also, Fig. 15 shows the dependencies of the growth rates and frequencies of unstable perturbations for $\chi_n = 4$ and different values of χ_B.

V. CONCLUSIONS

We have presented a detailed analysis of the gradient drift electrostatic instabilities in partially magnetized plasmas with hot electrons and cold ions in crossed electric and magnetic fields. The azimuthal oscillations with $k_x \ll k_y$ driven by the equilibrium electron flows perpendicular to the magnetic field are considered. Two cases are analyzed separately: (1) the general case in which the equilibrium electron $\mathbf{E} \times \mathbf{B}$ velocity, V_E, is of the order of the magnetic drift velocity V_D or larger; (2) the case of negligibly weak electric field, $V_E \ll V_D$, in which the instability is driven by the electron magnetic drift velocity.

It is shown that in the general case of moderate and strong electric fields the character of instability depends on the ratio between the gradients of equilibrium plasma density and magnetic field. Minimizing the function $\xi(\chi_n, \chi_B, k)$ with respect to the wavenumber k, we have analytically found the critical value of the instability drive ξ_{cr} for all possible ranges of parameters χ_n and χ_B. The corresponding results are summarized in Figs. 2(a) and 2(b) as the dependencies $\xi_{cr} = \xi_{cr}(\chi_B)$ at fixed values of χ_n in two different cases of

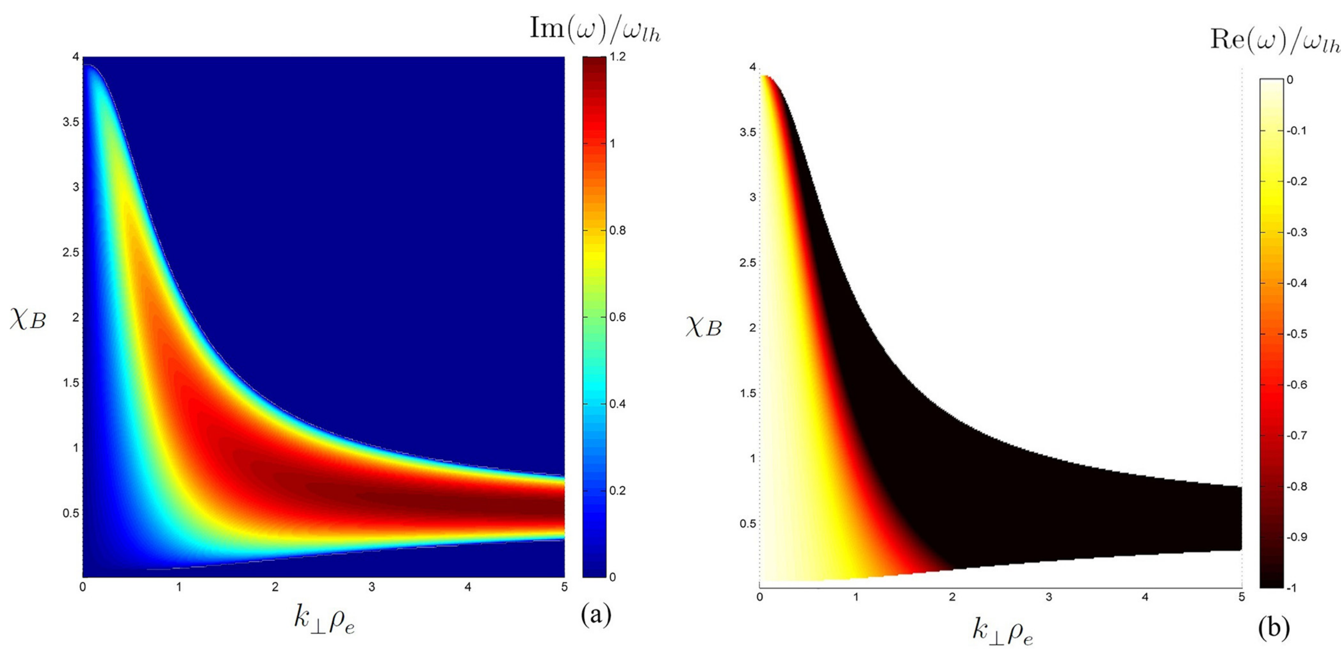

FIG. 14. Contour-plots of growth rates (a) and frequencies (b) of unstable modes in $k_\perp - \chi_B$-plane. Here $\chi_n = 4$. In (b), white color indicates the stable area, and modes with frequency higher than ω_{lh} are shown in black.

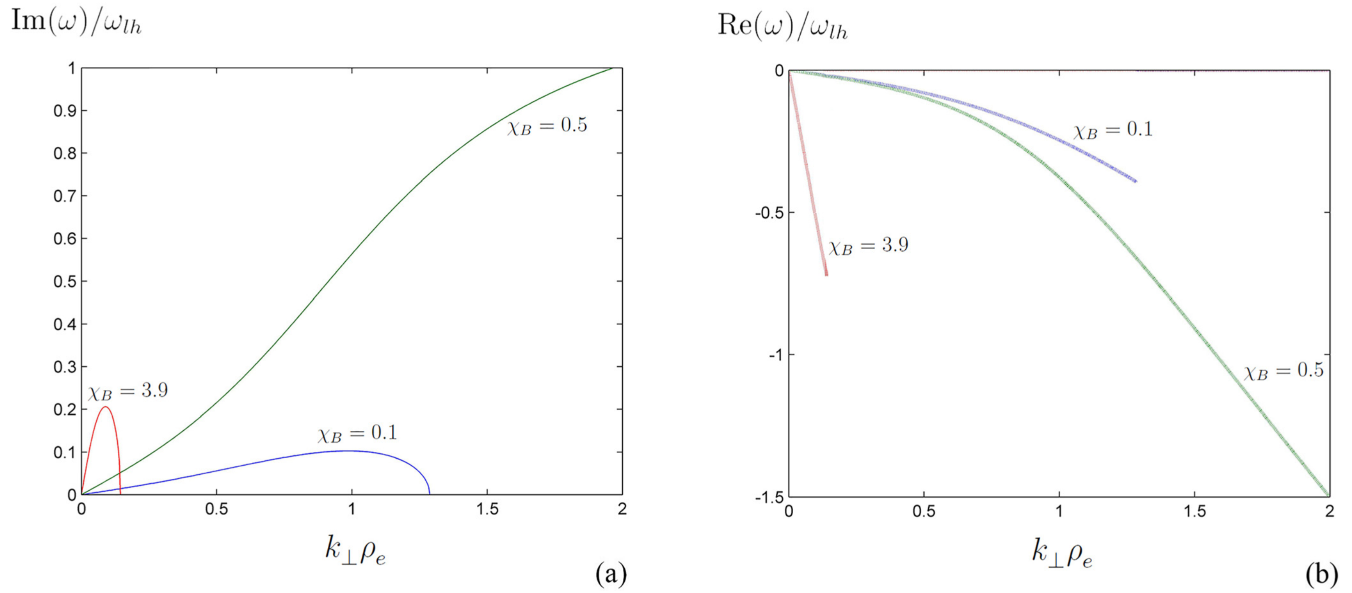

FIG. 15. Dependencies of growth rates (a) and frequencies (a) of unstable modes on wavenumber $k_\perp$. Different lines correspond to different values of χ_B: $\chi_B = 0.1$—near the lower critical value; $\chi_B = 3.9$—near the upper critical value; $\chi_B = 0.5$. Here, $\chi_n = 4$.

weak, $0 < \kappa_n\rho_s < 1$, and sufficiently strong, $\kappa_n\rho_s \gtrsim 1$, plasma density inhomogeneity. The values ξ_{cr} define the marginal stability condition. In accordance with the concept of the self-organized criticality of the anomalous transport, one could expect that due to the turbulent transport caused by gradient drift instability the plasma profile corresponding to the marginal stability $\xi = \xi_{cr}$ will establish. We have shown that the marginal stability condition essentially depends on the ratio between the gradients of equilibrium plasma density and magnetic field. It is important to note that the long-wavelength perturbations are unstable when $\xi > \xi_0$ (see Fig. 3) and such perturbations provide the dominant contribution to the anomalous transport. Therefore, one can expect that the marginal stability profile will be determined by long-wavelength perturbation with the condition $\xi = \xi_0$ or in terms of physical parameters

$$\left(\frac{eE_0}{T_e} + \frac{1}{B_0^2}\frac{dB_0^2}{dx}\right)\cdot\frac{B_0^2}{n_0}\frac{d}{dx}\left(\frac{n_0}{B_0^2}\right) = \frac{1}{4\rho_s^2}.$$

One can also speculate that the instability of long-wavelength low-frequency modes near the marginal stability boundary may be the origin for low-frequency structures often observed in Hall plasma devices.[10,21]

Other marginal stability boundaries are defined by the conditions $\xi = \xi_{1\pm}$ and $\xi = \xi_{2\pm}$ or

$$\frac{eE_0}{T_e} + \frac{1}{n_0}\frac{\partial n_0}{\partial x} = \pm\frac{1}{\rho_s}$$

and

$$\frac{eE_0}{T_e} + \frac{1}{B_0^4}\frac{\partial B_0^4}{\partial x} = \pm\frac{1}{\rho_s}\sqrt{\frac{2\kappa_B}{\kappa_n - 2\kappa_B}}.$$

Near these boundaries, the short-wavelength perturbations are unstable which are less effective in producing anomalous transport. One can note that in the near anode region of a classical Hall thruster SPT-100 typical experimental data show that $\kappa_n/2 < \kappa_B < \kappa_n$ (the typical magnetic field and density profiles are presented, e.g., in Ref. 5). Under these conditions, the high-frequency, short-wavelength perturbations are unstable near the marginal stability boundary. The detailed comparison of our theoretical results with the actual experimental plasma profiles for the various Hall plasma devices is still required and it is planned for subsequent studies.

The dependencies of the frequencies and the growth rates of unstable oscillations are studied numerically and analytically (for some limiting cases) for fixed values of the gradients of equilibrium plasma density and magnetic field belonging to all possible intervals. It is shown that one can expect low-frequency ($\omega \ll \omega_{lh}$), long-wavelength oscillations with $k \to 0$ excited near the marginal stability boundary, at $\xi \approx \xi_{cr} = \xi_0$. One may expect such a situation in the regions of sufficiently large gradients of magnetic field magnitude, $|\kappa_B|\rho_s \gg 1$. In the regions with weak plasma density gradient ($0 < \kappa_n\rho_s < 1$), such modes can have place only when $\chi_B \in]-\infty, \chi_n - 1/2]$ or $\chi_B \in [\chi_n + 1/2, \infty[$. Meanwhile, in the regions with strong plasma density gradient ($\kappa_n\rho_s \geq 1$), these modes may exist when $\chi_B \in]-\infty, \chi_B^{(-)}]$, $\chi_B \in [\chi_n - 1/2, \chi_B^{(+)}]$, or $\chi_B \in [\chi_n + 1/2, \infty[$. In this case, the shorter-wavelength oscillations are effectively suppressed even by the small, $k_\perp\rho_e \ll 1$, electron FLR effects [see Eq. (31)]. For larger values of ξ, which are also appropriate to standard Hall-type thrusters, there are always the unstable high-frequency oscillations with $\omega \gtrsim \omega_{lh}$. The larger the ξ, the larger the growth rate. Besides that, for large ξ, only the long-wavelength oscillations are unstable due to the suppression of instability of shorter-wavelength oscillations by the electron inertia effects[14] [see Eqs. (37) and (38) and Fig. 5]. It is also shown that for a special value of ξ defined by $\xi = \pm 1 - \chi_B$ and χ_B outside the interval $[\chi_n/2, \chi_n]$ the whole spectrum of oscillations is unstable. The maximal growth rate is achieved for the high-frequency ion-sound mode [Eq. (36)]. For $k_\perp \to \infty$, the growth rate asymptotically goes to the value described by Eq. (36), which does not depend on $k_\perp$.

In the case of negligibly weak electric field, the instabilities are driven by the electron magnetic drift flow V_D. Such conditions can arise outside of the exit plane of Hall thruster and in other laboratory cross-field devices if the electric field changes sign inside the plasma channel (see, e.g., the magnetron discharge profiles from Ref. 11). We have rigorously proved that such instability can take place only in the regions with significantly strong plasma density gradients such that $\chi_n \gtrsim 1$ and if $\left(|V_{\star e}| - \sqrt{V_{\star e}^2/c_s^2 - 1}\right)/2 < |V_D| < (|V_{\star e}| + \sqrt{V_{\star e}^2/c_s^2 - 1})/2$. We have shown that for $|V_D| = c_s/2$ the whole spectrum of perturbations with $0 < k_\perp < \infty$ is unstable.

We have determined that the long-wavelength, low-frequency instability exists only when the amplitude of electron magnetic drift velocity $|V_D|$ is close to the lower critical value, $|V_D| - V_{cr}^{(-)} \ll c_s^2/\sqrt{V_{\star e}^2/c_s^2 - 1}$. Otherwise, the shorter-wavelength high-frequency ($\omega \sim \omega_{lh}$ and higher) oscillations with much larger growth rates are excited.

ACKNOWLEDGMENTS

This work was supported in part by the Russian Science Foundation (Project No. 17–12-01470). V.I.I. appreciates the financial support from the Ministry of Education and Science of the Russian Federation (Agreement Nos. 02.A03.21.0008 and 3.2223.2017).

[1]Y. V. Esipchuk and G. N. Tilinin, Sov. Phys. Tech. Phys. **21**, 417 (1976).
[2]D. Tomilin, Phys. Plasmas **20**, 042103 (2013).
[3]V. D. Nikitin, D. Tomilin, A. Lovtsov, and A. Tarasov, Europhys. Lett. **117**, 45001 (2017).
[4]W. Frias, A. I. Smolyakov, I. D. Kaganovich, and Y. Raitses, Phys. Plasmas **19**, 072112 (2012).
[5]W. Frias, A. I. Smolyakov, I. D. Kaganovich, and Y. Raitses, Phys. Plasmas **20**, 052108 (2013).
[6]A. I. Smolyakov, O. Chapurin, W. Frias, O. Koshkarov, I. Romadanov, T. Tang, M. Umansky, Y. Raitses, I. D. Kaganovich, and V. P. Lakhin, Plasma Phys. Controlled Fusion **59**, 014041 (2017).
[7]A. Kapulkin and M. M. Guelman, IEEE Trans. Plasma Sci. **36**, 2082 (2008).
[8]E. Y. Choueiri, Phys. Plasmas **8**, 1411 (2001).
[9]J.-P. Boeuf, J. Appl. Phys **121**, 011101 (2017).
[10]E. Chesta, C. Lam, N. Meezan, D. Schmidt, and M. Cappelli, IEEE Trans. Plasma Sci. **29**, 582 (2001).
[11]T. Ito, C. V. Young, and M. A. Cappelli, Appl. Phys. Lett. **106**, 254104 (2015).
[12]C. L. Ellison, Y. Raitses, and N. J. Fisch, Phys. Plasmas **19**, 013503 (2012).
[13]O. A. Gorshkov, D. A. Tomilin, and A. A. Shagaida, Plasma Phys. Rep. **38**, 271 (2012).
[14]V. P. Lakhin, V. I. Ilgisonis, A. I. Smolyakov, E. A. Sorokina, and N. A. Marusov, Phys. Plasmas **25**, 012106 (2018).
[15]V. P. Pastukhov, Sov. J. Plasma Phys. **6**, 549 (1980).
[16]V. V. Piterskii, V. P. Pastukhov, M. S. Ioffe, B. I. Kanaev, and E. E. Yushmanov, Sov. J. Plasma Phys. **14**, 94 (1988).
[17]V. I. Ilgisonis and V. P. Pastukhov, Transversal electron losses in magneto-electrostatic traps with low pressure of plasma, Preprint IAE-3495/6 (1981).
[18]J. J. Ramos, Phys. Plasmas **12**, 112301 (2005).
[19]A. B. Mikhailovskii and V. S. Tsypin, Sov. Phys. JETP Lett. **3**, 158 (1966).
[20]A. B. Mikhailovskii, *Theory of Plasma Instabilities: Volume 2: Instabilities of an Inhomogeneous Plasma* (Consultants Bureau, New York, 1974), Vol. 2.
[21]A. I. Morozov, Y. V. Esipchuk, A. M. Kapulkin, V. A. Nevrovskii, and V. A. Smirnov, Sov. Phys. Tech. Phys. **17**, 482 (1972).